© 2014. Published by The Company of Biologists Ltd | Development (2014) 141, 1503-1513 doi:10.1242/dev.101436

RESEARCH ARTICLE

Sub-circuits of a gene regulatory network control a developmental epithelial-mesenchymal transition

Lindsay R. Saunders and David R. McClay*

ABSTRACT

Epithelial-mesenchymal transition (EMT) is a fundamental cell state change that transforms epithelial to mesenchymal cells during embryonic development, adult tissue repair and cancer metastasis. EMT includes a complex series of intermediate cell state changes including remodeling of the basement membrane, apical constriction, epithelial de-adhesion, directed motility, loss of apical-basal polarity, and acquisition of mesenchymal adhesion and polarity. Transcriptional regulatory state changes must ultimately coordinate the timing and execution of these cell biological processes. A well-characterized gene regulatory network (GRN) in the sea urchin embryo was used to identify the transcription factors that control five distinct cell changes during EMT. Single transcription factors were perturbed and the consequences followed with *in vivo* time-lapse imaging or immunostaining assays. The data show that five different sub-circuits of the GRN control five distinct cell biological activities, each part of the complex EMT process. Thirteen transcription factors (TFs) expressed specifically in pre-EMT cells were required for EMT. Three TFs highest in the GRN specified and activated EMT (alx1, ets1, tbr) and the 10 TFs downstream of those (tel, erg, hex, tgif, snail, twist, foxn2/3, dri, foxb, foxo) were also required for EMT. No single TF functioned in all five sub-circuits, indicating that there is no EMT master regulator. Instead, the resulting sub-circuit topologies suggest EMT requires multiple simultaneous regulatory mechanisms: forward cascades, parallel inputs and positive-feedback lock downs. The interconnected and overlapping nature of the sub-circuits provides one explanation for the seamless orchestration by the embryo of cell state changes leading to successful EMT.

KEY WORDS: Gene regulatory network, Epithelial-mesenchymal transition, Sea urchin, Snail, Twist

INTRODUCTION

During development, epithelial-mesenchymal transition (EMT) occurs during gastrulation to create mesoderm, and in many vertebrates, endoderm separates from the epiblast by EMT. EMTs are also used many times during organogenesis and at later stages of development (Shook and Keller, 2003). EMT continues to be important throughout adult life for tissue maintenance and wound healing but can also be detrimental in a cancerous environment that contributes to metastasis (Yang and Weinberg, 2008). Many studies have demonstrated that EMT is a complex series of cell state changes that include apical constriction of cells, basement membrane remodeling, adherens junctions break down, cell-cell adhesion loss, apical-basal polarity loss, motility acquisition and other changes (Levayer and Lecuit, 2008; Acloque et al., 2009; Kalluri and Weinberg, 2009; Thiery et al., 2009). Understanding how this complex morphogenetic movement is controlled has proven challenging.

Expression profiling and overexpression studies have produced a wealth of data about the molecular drivers of EMT, most notably the TGFβ signaling pathway (Moustakas and Heldin, 2012) and the Snail, Twist and ZEB families of transcription factors (TFs) (Sánchez-Tilló et al., 2012). Snail and twist were first characterized in *Drosophila melanogaster* where they were shown to be necessary for mesoderm and ventral furrow formation (Anderson and Nusslein-Volhard, 1984; Simpson, 1983), and later discovered to be integral for EMTs (Oda et al., 1998). These transcription factors were then discovered in vertebrates (Sargent and Bennett, 1990; Hopwood et al., 1989) where expanded genomes included families of genes: SNAI1 (Snail, Snail1, Sna), SNAI2 (Snail2, Slug), SNAI3 (Snail3, Smuc), TWIST1 (Twist), TWIST2, ZEB1 (BZP) and ZEB2 (SIP-1). The case of SNAI3 is still slightly ambiguous (Kataoka et al., 2000; Bradley et al., 2013), but these TFs are all considered to be E-cadherin repressors and have been proposed to be the 'master regulators' that are capable of inducing the full EMT program (Zheng and Kang, 2013).

If the master regulatory control hypothesis were correct, snail or another master regulator would control all of the contributing components of EMT. Snail and twist have been shown to directly repress transcription of E-cadherin (Batlle et al., 2000; Cano et al., 2000; Vesuna et al., 2008) and snail upregulation destabilizes adherens junctions (Kim et al., 2013). Based on evidence that snail and twist increase cancer cell invasiveness, it has been proposed that they may also participate in basement membrane remodeling and motility, and this has fueled additional interest in their potential role as master regulators. However, this support of a master regulatory model is based on overexpression of snail and twist (Naber et al., 2013; Lee et al., 2006), and overexpression studies often have interpretation problems.

Ultimately, the control mechanism of EMT must be contained within a gene regulatory network (GRN), as all activities of the cell are initially regulated by transcriptional control of gene expression. Predictive EMT GRN models have been produced from data on temporal TF activity changes (Siletz et al., 2013), and these lend support to the hypothesis that the control of EMT is coordinated by a GRN. Here, we take this prediction an important step further and directly test GRN states for control of EMT.

To observe regulatory control of EMT directly, we used the sea urchin *Lytechinus variegatus*, a deuterostome and close vertebrate relative (Turbeville et al., 1994). Early specification in the sea urchin was the subject of intense study to build GRNs that define how each cell lineage is transcriptionally programmed (Davidson et al., 2002; Rafiq et al., 2012). Each node in that GRN is built on perturbation data, and many node connections have been authenticated by cis-regulatory analysis to confirm direct inputs. Intelligent manipulation of GRN states is possible where a GRN is first experimentally

Department of Biology, Duke University, Durham, NC 27708, USA.

*Author for correspondence (dmcclay@duke.edu)

Received 18 July 2013; Accepted 3 February 2014

Development (2014) doi:10.1242/dev.101436

validated and the logic of TF interactions is known. In this regard, the sea urchin GRN is advantageous over a predictive GRN based on database inferences. The topology of the sea urchin GRN encapsulates all known direct developmental TF interactions and therefore provides an excellent resource for analysis of EMT control.

The first cells in *L. variegatus* to undergo EMT are the primary mesenchyme cells (PMCs) that are descendants of micromeres, the smallest cells of an unequal fourth cleavage. At 8.5 hours post fertilization (hpf) the posterior end of the embryo thickens as PMC precursors elongate via apical constriction. This first morphological sign of the impending EMT is followed by the appearance of the first mesenchymal PMCs at 9 hpf. Over a period of 45 minutes, a total of 32 PMCs complete EMT, move into the blastocoel, divide once and migrate away from the ingression site to form a ring where they will eventually synthesize the larval skeleton (Ettensohn, 1990).

Here, we have developed assays to follow the dynamics of EMT using a combination of live imaging and immunostaining. To understand the role of the GRN transcription factors in controlling EMT, we systematically perturbed each transcription factor that was expressed by the PMCs 1-2 hours prior to EMT plus three TFs upstream of those. We chose the proximal 13 TFs as regulatory control candidates. Each of the 13 TFs were knocked down, and each perturbation was observed to impact distinct components of EMT. Assays were designed to directly observe the intermediate cell state changes that contribute to EMT. When the perturbations were mapped onto the GRN, five distinct sub-circuits controlled basement membrane remodeling, motility, apical constriction, apical-basal polarity and de-adhesion. Although all TFs were independently required to complete EMT, no single TF was required in all five sub-circuits. Each of the three upstream TFs was required for distinct subcircuits rather than behaving as master regulators. Our results show for the first time the complex and interconnected regulatory program driving EMT in a developmental model organism.

RESULTS

Identification of the gene regulatory network (GRN) that controls EMT

We first delineated the GRN specifying the skeletogenic lineage in *L. variegatus*. This was very similar to that previously established for *S. purpuratus* (Oliveri et al., 2008) (Fig. 1). Perturbation analyses of all skeletogenic precursor genes were used to build the GRN model in the same way earlier GRNs in the sea urchin had been constructed (Davidson, et al., 2002; Davidson et al., 2006). The biggest difference between the current *S. purpuratus* GRN model and that shown in Fig. 1 is the observation that snail and twist are part of the *L. variegatus* GRN (Wu et al., 2007; Wu et al., 2008). As specification of the skeletogenic GRN occurs prior to EMT, the network depicted in Fig. 1 must include transcription factors that control the process of EMT. Therefore, in constructing the skeletogenic GRN, we took careful note of time of first expression of each transcription factor. We reasoned that transcription factors activated within 1 or 2 hours prior to the beginning of EMT were the candidates most likely to provide the proximal control of that process. Indeed, preliminary perturbations indicated that most, if not all, knockdowns of transcription factors in that group had an EMT phenotype. Specifically, 10 transcription factors shown in Fig. 1 fit these criteria and were subjected to further analysis (detailed below). We then extended the analysis to three transcription factors expressed upstream of the 10, each modeled to be necessary for expression of one or more of the 10 downstream transcription

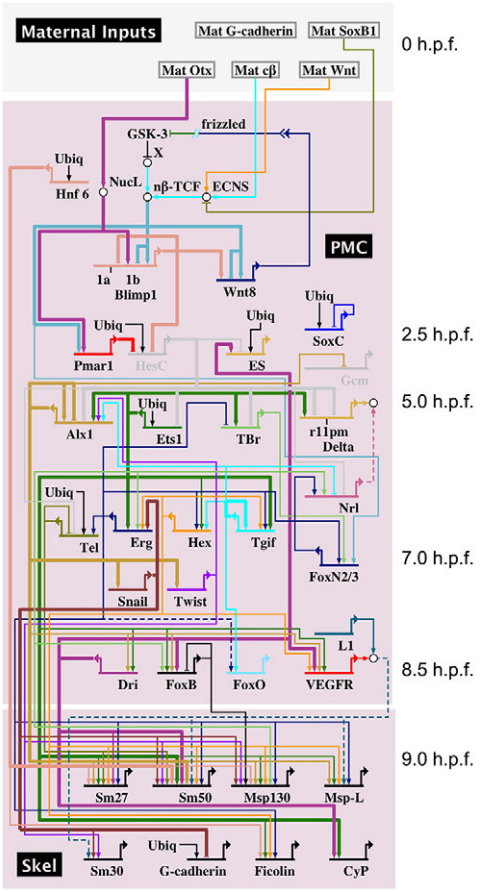

Fig. 1. *Lytechinus variegatus* skeletogenic cell gene regulatory network. This gene regulatory network (GRN) models the first 9 hours of development of the skeletogenic cells. An approximate time-line is given top to bottom on the right. At the top four maternal inputs activate the GRN at about 2.5 hours (the time of the unequal 4th cleavage that produces the micromeres which are the skeletogenic precursors). The group of genes activated between 7 and 8.5 hpf are the transcription factors expressed proximal to EMT (tel, erg, hex, tgif, foxN2/3, snail, twist, dri, foxB, foxO). Three transcription factors expressed upstream of those 10, and with direct or indirect input into all 10, include alx1, ets1 and tbr. As modeled, each gene is represented by a horizontal bar with the name of the gene under the bar. The bar represents the cis regulatory region of the gene. An arrow of the same color as the bar represents the mRNA/protein output of that gene. If the output arrow terminates with an arrowhead, the transcription factor serves as an activator. If the output terminates with a 90° line, the transcription factor is modeled to function as a repressor. Inputs arriving vertically onto a gene bar represent modeled cis-regulatory inputs that either activate or repress transcription of the gene. Genes listed in the bottom two lines are effector genes involved in differentiation of the skeletogenic cells.

factors. Having defined those transcription factors most likely to be involved in regulating EMT in the PMCs, we then systematically knocked down each of the 13 transcription factors, one at a time, to ask how each affected EMT. For each transcription factor tested, two morpholinos were identified and in the preliminary tests each pair had identical phenotypic outcomes. We developed methods to separately analyze basement membrane remodeling, acquisition of motility, cell shape change, cell polarity and de-adhesion, each a component function of EMT. The data were quantified from 20+ independent assessments of each transcription factor knockdown compared with controls. Each assay and its outcome are described below.

Development (2014) doi:10.1242/dev.101436

Basement membrane remodeling

An early and important EMT event is passage through the basement membrane. To highlight its importance, the basement membrane may be more than just a physical barrier as laminin, a major basement membrane component, has been shown to suppress EMT (Chen et al., 2013). To determine whether and when the basement membrane is degraded in the urchin embryo, we monitored laminin staining in a control time-course from 6 hpf, 3 hours before EMT begins, to 10 hpf. Fixed control embryos were double immunostained with anti-laminin and anti-1D5, a PMC-specific marker (Fig. 2A,A′). The laminin antibody stained a uniform basement membrane meshwork beneath the epithelial cells of the blastula (Fig. 2B); the same pattern as previously shown in *S. purpuratus* (Benson et al., 1999). About 30 minutes prior to appearance of the first mesenchymal PMCs, a laminin-free hole appeared basal to the PMC precursors (Fig. 2C). At the onset of EMT the hole diameter exactly encircled the nascent PMCs (Fig. 2D). To determine which TFs were necessary for laminin hole production, each TF candidate (alx1, ets1, tbr, tel, erg, tgif, hex, twist, snail, foxn2/3, dri, foxb and foxo) was knocked down and embryos fixed with matched controls at 10 hpf after EMT completion; embryos were then immunostained with anti-laminin, anti-1D5 and Hoechst's (Fig. 2G-S). In total, 132 embryos were analyzed by confocal microscopy, including 24 control embryos and an average of nine embryos per knockdown. Knockdowns for 10 TFs produced a laminin hole comparable with controls by 10 hpf as measured by comparing lateral and vegetal fluorescent intensity differences against that of controls (Fig. 2T). Three TF knockdowns showed no hole in laminin staining compared with controls: tbr, dri and hex (Fig. 2G-I,T). These three TFs do not regulate each other but regulate the appearance of the laminin hole in parallel and this was reflected in the sub-circuit for basement membrane remodeling (Fig. 7A).

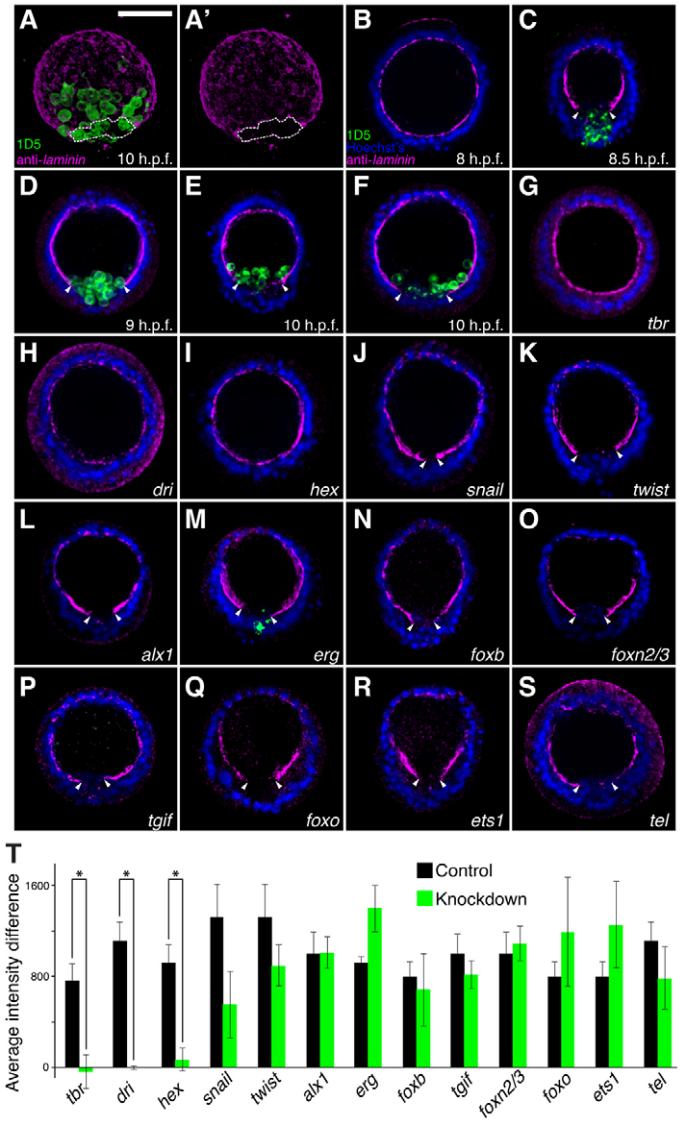

Fig. 2. Basement membrane remodeling. (A,A′) 3D projection of confocal images. At 10 hpf, anti-1D5 (green) stains blastocoelar PMCs (A) that have completed EMT. Anti-laminin (magenta) stains BM meshwork (A′) but is absent from a large posterior hole. Dotted outlines show the laminin hole. Scale bar: 50 µm. (B-S) Confocal projections (20 µm) of anti-laminin (magenta) and 1D5 (green) immunostaining with Hoechst's (blue). Control time course (B-F) and 10 hpf. TF knockdowns (G-S). Embryos without tbr, dri and hex (G-I) did not make a laminin hole. Arrowheads indicate laminin holes. (T) Difference between lateral and vegetal pixel intensity distinguishes small random meshwork holes from laminin holes. *Significant difference between TF and paired control indicates random meshwork in knockdown without laminin hole, $P<0.01$. Error bars show s.e.m.

In vivo time-lapse observation of EMT

The 32 skeletogenic cells of the transparent sea urchin embryo undergo EMT over 45 minutes beginning at about 8.5 hpf. The precise timing of this EMT and the optical clarity of the embryo provided the system for a dynamic analysis of the process. For this assay, the three upstream TFs and nine proximal candidate TFs shown by control experiments to be necessary for EMT (alx1, ets1, tbr, twist, snail, tel, erg, tgif, hex, foxn2/3, foxb and foxo) were separately knocked down with morpholino antisense oligos or mRNA encoding dominant-negative protein (supplementary material Table S3) (dri knockdown movies did not meet our minimum criteria to be included in statistical analyses, i.e. in focus for at least 1 hour after EMT of internal control PMCs, and therefore only the basement membrane phenotype of dri is reported here). To optimize the analysis, fertilized eggs were injected with two markers, a membrane green fluorescent protein label (mem-GFP) and a nuclear red fluorescent protein label (H2B-RFP), plus a control knockdown or a TF knockdown. At 2.5 hpf, one injected micromere was microsurgically transplanted onto an unperturbed 16-cell host embryo in place of one control micromere (Fig. 3A). That micromere averages 10 progeny: eight PMCs and two primordial germ cells. We imaged the embryos using *in vivo* time-lapse fluorescent microscopy beginning at the first morphological sign of EMT (thickened posterior epithelium) and ending 1 hour after EMT completion (control PMCs freely moving within the blastocoel) for two hours total (Fig. 3B-O; supplementary material Movies 1-14). At least 20 embryos for each knockdown were time-lapse recorded independently and from multiple parental crosses.

Labeled control transplant PMCs completed EMT at the same time as internal control PMCs from the host indicating the microsurgery itself did not delay EMT. TF knockdown PMCs were generally delayed and either did not complete EMT on time, or at all, and we observed several different phenotypes using this assay. Some TF knockdowns seemed to be more 'active' and pulled basally away from the epithelium. Other TF knockdowns appeared still or to be passively bumped around as the control PMCs exited the epithelium. We also observed several differences in the cell shape of different knockdowns. In order to evaluate these observed phenotypic differences as quantitatively and as objectively as

Development (2014) doi:10.1242/dev.101436

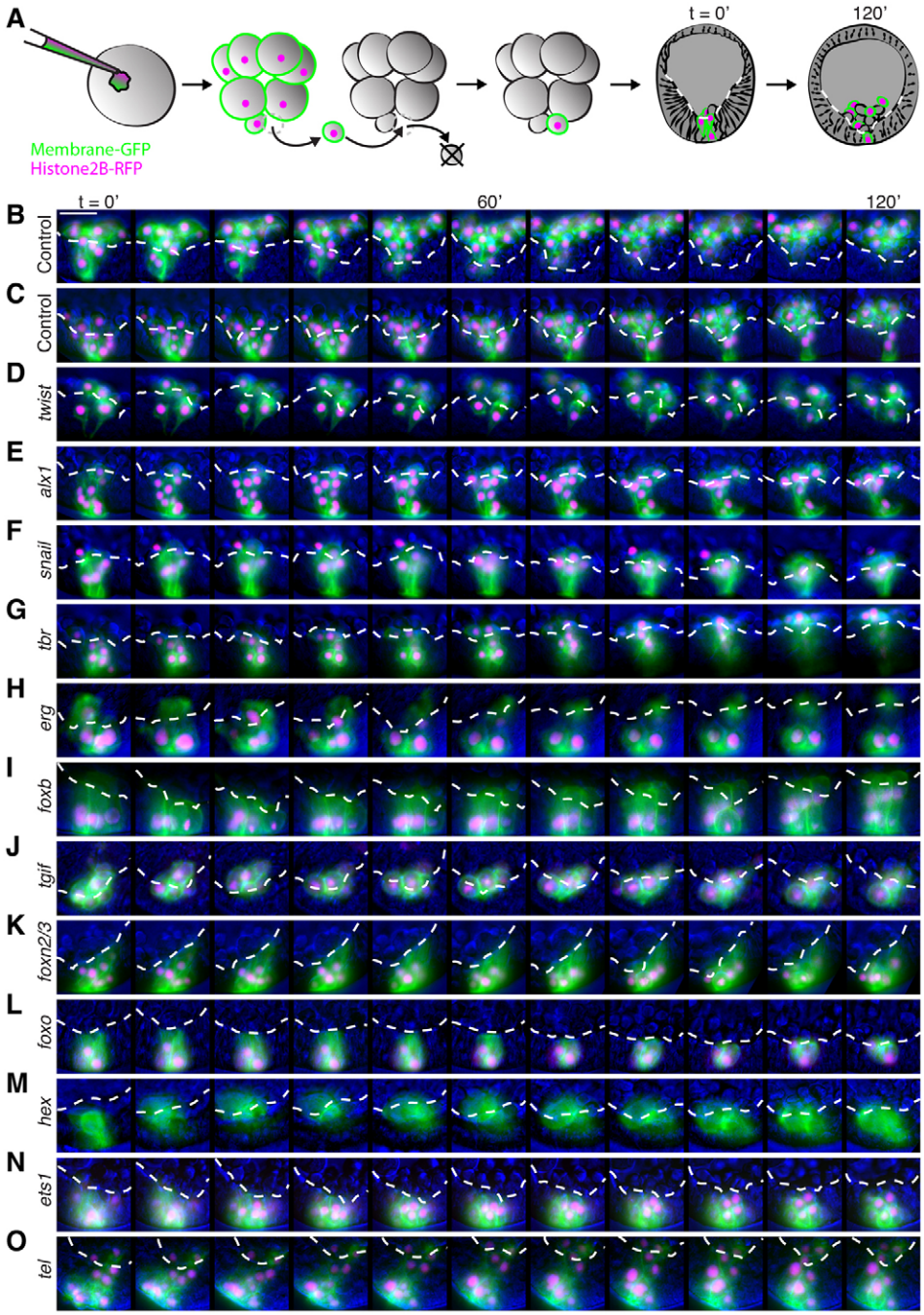

Fig. 3. *In vivo* time-lapse shows distinct EMT phenotypes. (A) Illustration of assay. Embryos were injected with one TF knockdown and two fluorescent markers: mem-GFP and H2B-RFP. At the 16-cell stage, one labeled micromere was transplanted to an unlabeled 16-cell host in place of one removed micromere. Embryos were imaged from the first morphological indication of EMT: a thickened posterior epithelium. Time-lapse duration from time t=0′ to 120′, time measured in minutes. (B-O) Time-lapse series of labeled PMCs for control (B), where PMCs but not presumptive germ cells were in focus, and control (C), where both PMCs and presumptive germ cells can be seen, and TF knockdowns twist (D), alx1 (E), snail (F), tbr (G), erg (H), foxb (I), tgif (J), foxn2/3 (K), foxo (L), hex (M), ets1 (N) and tel (O). Elapsed time in 12-minute intervals; dotted line indicates BM boundary. Scale bar: 20 µm.

possible, we designed separate statistical analyses to classify the phenotypic differences from each knockdown.

Motility or directional displacement

We developed a simple statistical image analysis to score motility of knockdowns as a displacement relative to landmark data (Fig. 4). The basement membrane, which demarcates the epithelial-blastocoelar boundary, served as our landmark and was manually segmented for each frame of each time-lapse movie (Fig. 4A,B). An initial concern was that experimental cells carrying TF knockdowns affecting laminin degradation would never cross the basement membrane boundary, regardless of motile ability. However, in the time-lapse assay, control cells outnumbered test cells 3:1 and those controls were able to remodel basement membrane; the time-lapse assay therefore effectively uncoupled motility from basement membrane degradation.

Movies were scored for directional displacement of cells across the landmark to record both the relative movement of cell mass and the relative position of cell nuclei. The data from this analysis showed a strong correlation between cell area distribution and nuclear position across the basement membrane boundary over EMT duration (Fig. 4C). For control cells, the area within the epithelium decreased 25.3% over 2 hours, ending with 32.5% average epithelial cell area after EMT completion. The control cell area remaining in the epithelium represented micromere descendants that were presumptive primordial germ cells, not PMC precursors, and therefore we did not expect the control measurements to reach 0% within the epithelium, regardless of timing. In addition, for

Development (2014) doi:10.1242/dev.101436

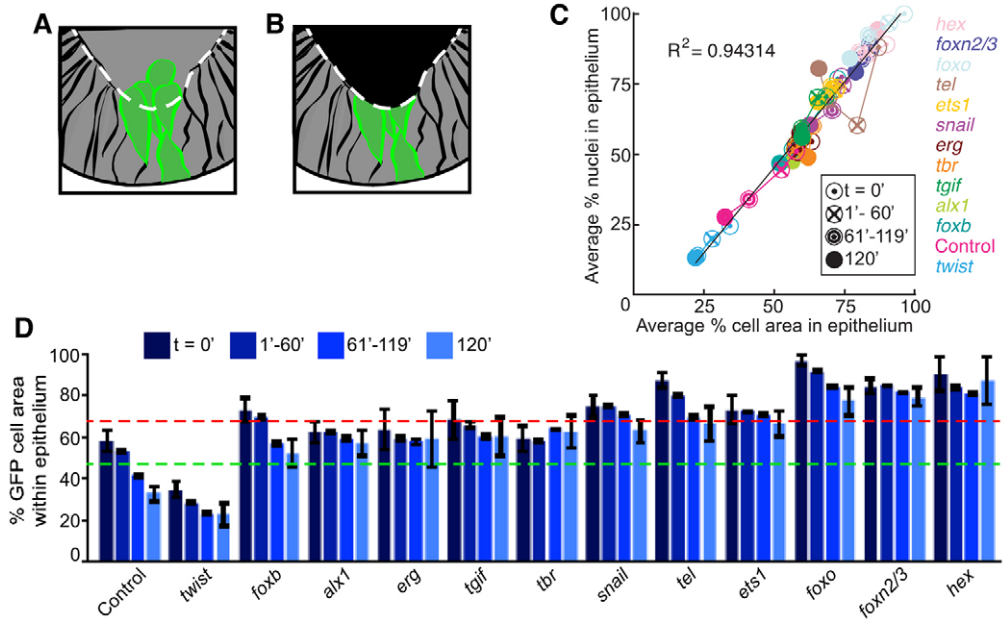

Fig. 4. Analysis of directional displacement. (A) Illustration of total GFP cell area. White dashed line represents BM boundary. (B) Illustration of epithelial GFP cell area. Black area represents blastocoel. (C) Percentage of cell area versus nuclei across the BM boundary is tightly correlated, time (t) is in minutes. R^2=0.94314. (D) Average percentage of GFP cell area within epithelium shows displacement over time. Green dashed line represents mean control displacement and red dashed line represents +1 SD from control. Time (t) is in minutes. Error bars show s.e.m.

technical reasons we started the time-lapse recording as soon as we saw vegetal plate thickening, and at that time the movies showed that the control cells had already partially protruded through the basement membrane. Of the 12 TF knockdowns, nine had some directional displacement and finished the time course with fewer nuclei and a reduced cell area within the epithelium within one standard deviation (SD) of pre-EMT controls (Fig. 4D). Three TF knockdowns (foxn2/3, hex and foxo) showed little or no displacement per movie and epithelial cell area averaged greater than 1 SD of pre-EMT controls over the duration of the time course (Fig. 4D). Other TFs may contribute to migratory movement after becoming mesenchymal, but with each knockdown preventing a full mesenchymal phenotype, this could not be assayed. The most conservative conclusion is that each of three TFs is necessary for initial motility required to exit the epithelium during EMT. Foxn2/3, hex and foxo have no regulatory relationships with one another and when mapped as a sub-circuit of the Lv PMC GRN they control motility via parallel inputs (Fig. 7B). These data suggest that components of motility are independently regulated by foxn2/3, hex and foxo.

Cell shape change and polarity change

We determined TFs affecting cell shape change by analyzing shape data for 7783 cells for 328 time-lapse movies using manually segmented individual cell mem-GFP outlines of transplanted PMCs. In order to control for the inclusion of presumptive germline cells from this shape analysis (because those cells do not undergo EMT with PMCs), the segmentation was limited to four of the larger cells with the most basal nuclear position for each movie, and excluded the two smallest cells with the most apical nuclear position. Outlines were elliptical Fourier transformed to the first 20 harmonics and normalized for apical-basal directionality. The subsequent principal component analysis described EMT cell shape phenotypes for the data set; the first three principal components explained 86% of the total shape variation (Fig. 5).

The mean shape within the dataset was slightly elongated with cytoplasmic polarization toward the basal end. Principal Component 1 (PC1) described shape variation along the apical-basal axis and ranged from least circular (circularity measurement of 0.38, elongated with a thin apical tail, −2 SDs from the mean shape) to most circular (circularity measurement of 0.90, +2 SDs from the mean) (Fig. 6A). PC2 described the lateral asymmetry of cells with no significant variation between controls and knockdowns (supplementary material Fig. S1). PC3 described variation between apical-basal polarities, ranging from a short apical tail with cytoplasm polarized basally to cytoplasm polarized apically (supplementary material Fig. S2).

Average PC1 and PC3 scores for control cells reflected the average apical constriction at time zero, i.e. morphological EMT initiation. The controls dramatically changed shape over the time-course, eventually becoming a rounded mesenchymal shape as EMT reached completion (Fig. 6B). Alx1 and snail knockdowns showed apical constriction with a long tail with PC1 scores similar to controls at time zero but, unlike control cells, they remained apically constricted throughout the time-course (Fig. 6A,B). Twist knockdowns showed apical constriction similar to alx1 and snail but with a shorter tail as described by PC3 (Fig. 6B; supplementary

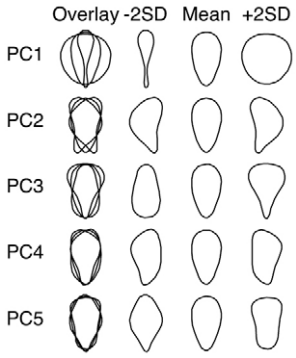

Fig. 5. Contours of principal component analysis. The first three PCs represent 86% of the total shape variation. The mean shape is ovoid, elongated along the apical-basal axis, and cytoplasm is slightly polarized to the basal side of the cell. PC1 represents variation from long apical constriction, −2 SD (standard deviation), to circular, +2 SD. PC2 represents lateral asymmetry. PC3 represents cytoplasm distribution along the apical-basal axis from polarized apically, −2 SD, to polarized basally with minor apical constriction, +2 SD.

Development (2014) doi:10.1242/dev.101436

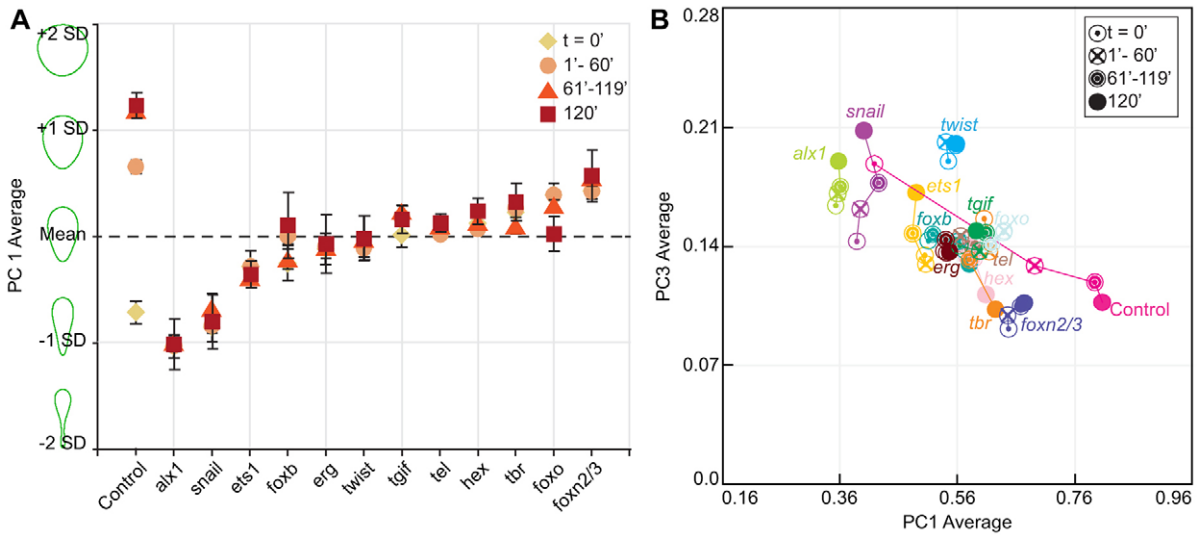

Fig. 6. Analysis of time-lapse data. (A) PC analysis of PMC shape data from 0′-120′, time in minutes. PC1 described shape variation from full apical constriction, −2 SD, to rounded, +2 SD. Error bars represent s.e.m. (B) PC1 versus PC3 shows average individual cell shape change in TF knockdowns over time. Snail, alx1 and twist cell shapes for all time points correspond to the time (t)=0′ control cell shape. Foxn2/3 cell shapes for all time points and tbr at end of time-lapse both correspond to later control cell shapes, 1′-120′. All other knockdowns cluster around the mean shape. Time (t) is in minutes.

material Fig. S2). PC1 scores for ets1, tel, erg, tgif, hex, foxb and foxo fell closest to the mean shape, corresponding most closely to an intermediate control cell shape, with no significant apical constriction and little change over time (Fig. 6A). PC3 scores for most TF knockdowns showed slightly more basal cytoplasm, a polarized distribution that resembled controls at time zero, but unlike controls did not change over the time-course (supplementary material Fig. S2). When PC1 and PC3 are considered together, most TFs (ets1, tel, erg, tgif, hex, foxb and foxo) lie on an overall median shape along an arrested trajectory of the control in the midst of shape change (Fig. 6B). Foxn2/3 was the only knockdown with a non-apically constricted shape significantly different from the mean shape for the duration of the time-course. Specifically, foxn2/3 had the most rounded PC1 score and the least polarized PC3 score (the most mesenchymal shape of any knockdown). Both foxn2/3 and tbr (which drives foxn2/3) had this more mesenchymal shape by the end of the time-course, indicating a loss of apical-basal polarity without EMT completion, i.e. a defect in maintaining the polarity required to exit the epithelium (Fig. 6B). We mapped these results onto the Lv PMC GRN as two sub-circuits controlling separate EMT cell changes: apical constriction, a complex forward cascade (Fig. 7C); and apical-basal polarity, a simple forward cascade (Fig. 7D).

De-adhesion

Arguably the best-studied EMT event is de-adhesion from the epithelium. De-adhesion begins with adherens junctions disassembly and continues with cell membrane turnover; the membrane loses cadherins and catenins, and adds mesenchymal adhesion molecules with extracellular matrix affinity (D'Souza-Schorey, 2005; Yap et al., 2007; Thiery et al., 2009). In *L. variegatus*, alx1, twist and snail constitute a functional sub-circuit in the GRN that controls the repression and endocytosis of cadherin required for de-adhesion (Wu and McClay, 2007; Wu et al., 2008). Our analysis of both snail and twist knockdowns showed a failure of PMCs to complete EMT in spite of four other successful cell state changes: laminin hole creation (Fig. 2J-L), directional movement toward the blastocoel (Fig. 4D), full apical constriction (Fig. 6A,B), and properly maintained polarity (Fig. 5B; supplementary material Fig. S2). This confirmed the previously described role for snail and twist in the de-adhesion component in both this and other EMT models. Alx1, the known driver of both snail and twist expression (Wu and McClay, 2007; Wu et al., 2008), had the same knockdown phenotype as snail and twist, indicating alx1 is also required for de-adhesion. Therefore, alx1, twist and snail display control over adhesive state change and make a distinct sub-circuit of the GRN, a positive-feedback lockdown, that governs the de-adhesion process (Fig. 7E). This sub-circuit is inclusive only and does not exclude other TFs.

DISCUSSION

In these experiments, no single transcription factor controlled all five EMT cell state changes analyzed. Importantly, the three specifiers, alx1, ets1 and tbr, each controls expression of a different subset of the proximal TFs, and perturbation of each of these three specifiers has a different impact on EMT. Furthermore, each of the 13 transcription factors tested contributed to up to three of the cell biological properties scored, but was unnecessary for two or more of the properties. Thus, none of the TFs tested is a candidate for a master regulator of EMT.

In the sea urchin, the 13 EMT TFs studied here belong to eight different TF families (homeobox, TALE homeobox, ETS, t-box, snail, twist, forkhead box and ARID families). Additionally, 12 of the 13 TFs are the sole member of their subfamily represented in the sea urchin genome (only the FoxN subfamily has two members: foxn2/3 studied here and foxn1/4, which has not been studied). To compare this with vertebrates, a total of 30 human orthologs correspond to the 13 TFs studied here. All orthologs but hex (hhex) are found within a subfamily of two or three members. Only eight of the 30 orthologs have been reported to be involved directly in EMT regulation (supplementary material Table S3). The other 22 orthologs are expressed in various cell types that frequently undergo EMT, meaning those 22 are additional candidates for EMT regulation (supplementary material Table S3).

This raises the issue of relatedness between sea urchin and vertebrates, including humans, as to whether the other 22 orthologs have an undiscovered EMT function. Perhaps in many cases, vertebrate genome duplications have resulted in redundancy of EMT

Development (2014) doi:10.1242/dev.101436

Fig. 7. The unique sub-circuits that regulate individual EMT events. (A) The basement membrane remodeling sub-circuit is constructed of the parallel inputs tbr, hex and dri. (B) The motility sub-circuit is constructed of the parallel inputs hex, foxn2/3 and foxo. (C) The apical constriction sub-circuit is a complex forward cascade including ets1, tbr, erg and tgif and terminating with tel, hex, foxn2/3, foxb and foxo. (D) The apical-basal polarity sub-circuit is a simple forward cascade beginning with tbr and terminating into foxn2/3. (E) The de-adhesion sub-circuit uses positive-feedback lockdown where alx1 is in positive loop with twist and also promotes snail. (F) Each of the sub-circuits is combined into one circuit diagram. This integrated circuit shows with colored dotted lines the transcription factors that overlap in the several subcircuits. TF relationships are shown with terminal nodes into five color-coded EMT cellular behaviors: apical constriction (yellow), motility (red), apical-basal (AB) polarity (purple), de-adhesion (blue) and BM remodeling (green).

function within subfamilies. For example, our study is the first to link tgif directly to EMT. However, although tgif1 and tgif2 individual null mice are viable (Shen and Walsh, 2005; Powers et al., 2010), the double knockout fails to gastrulate, and even though these embryos properly downregulate E-cadherin, there is no transition to mesoderm (Powers et al., 2010). That phenotype is consistent with an intermediate arrest during EMT, not dissimilar to what we have shown for the sea urchin tgif knockdown.

In sea urchin, many of the TFs involved in EMT are expressed only for a short time window spanning from just before to just after EMT. Given this limited time frame of expression it is easy to understand how in candidate screens of vertebrate EMTs, TF homologs could easily be missed. Using tgif as an example again, neither tgif1 nor tgif2 transcripts have been detected in developing mouse embryos before gastrulation (Bertolino et al., 1996; Jin et al., 2005; Shen and Walsh, 2005), yet the double knockout fails to gastrulate (Powers et al., 2010).

Thus, it is quite possible the vertebrate EMT and the co-opted metastatic EMT, use some, if not all the TFs observed in sea urchin embryo EMT. This possibility remains to be tested. In the meantime, as many of the TFs seen in the mammalian system are part of the sea urchin EMT, and that embryonic EMT is easily manipulated by perturbing its transcriptional drivers, the sea urchin will continue to provide an excellent model system for more detailed analysis of the relationship of the cell biology controlled by those TFs.

Basement membrane remodeling

The basement membrane is a meshwork of macromolecules, which includes collagen and laminin, that must be penetrated by the nascent mesenchymal cells as they leave the epithelium during EMT (Levayer and Lecuit, 2008). In sea urchin, and in other systems, the means by which the PMCs (or other cells) break through the basement membrane has long been a focus of curiosity. One hypothesis was that the basement membrane meshwork is loose

Development (2014) doi:10.1242/dev.101436

enough that cells might force their way through mechanically, i.e. non-proteolytic remodeling (Wu and McClay, 2007; Rowe and Weiss, 2008). The more popular alternative model suggests that the basement membrane penetration is assisted by proteases, but there are data to support both models (Rowe and Weiss, 2008).

Many matrix metalloproteases (MMPs) are present in the sea urchin genome and a number are expressed by mesenchyme at, or near the time of, EMT (Angerer et al., 2006). Our data support the hypothesis that PMCs use proteolysis to breach the BM during EMT; morphants for 10 of the 13 TFs assayed successfully made holes in the laminin of the BM before the cells left the epithelium. Had the hole been produced by mechanical leveraging of the PMCs one would have expected to see cells passing through the hole as it formed. In addition, two of the motility-defective knockdowns (foxn2/3 and foxo) made a laminin hole without any potential mechanical force, because foxn2/3 and foxo knockdowns each lacked both apical constriction and motility, and did not move through the laminin hole that had been produced. Although a mechanical component cannot be ruled out entirely as a mechanism of breaching the basement membrane, the contrary evidence is convincing. The control hole has a diameter that exactly encompasses the diameter of the PMCs below it. Piling up of laminin around the circumference of the hole was not seen. Thus, it is likely the direct targets of the tbr, hex and dri are either proteases or activators of proteases.

Tbr, hex and dri have not been previously reported to play a role in basement membrane remodeling. However, several TF knockdowns that successfully degraded laminin in our model system have been shown to promote basement membrane remodeling in other systems. Previous studies have demonstrated that ets1 directly upregulates mmp1 (collagenase 1), mmp3 (stromelysin 1), mmp9 (gelatinase B) and mmp13 (collagenase 3) (Westermarck et al., 1997; Baillat et al., 2006; Ghosh et al., 2012). Snail and twist are also associated with upregulated MMPs (Sánchez-Tilló et al., 2012), although this evidence is indirect. It is possible that ets1, snail and twist are not required for laminin degradation, but instead promote proteolysis of other basement membrane macromolecules.

Motility

The motility sub-circuit we record is conservative, reflecting only those TFs crucial for the initial movement required to exit the epithelium and enter the blastocoel. Previous studies show that foxn2/3, hex and foxo are each expressed in different migrating tissue types. Our study confirms previous evidence that foxn2/3 is required for PMC migration in sea urchins (Rho and McClay, 2011). Foxn3 is required for cranial neural crest development, a highly motile cell type that undergoes EMT in *Xenopus laevis*, and is also required for proper craniofacial development in mice, which may also implicate neural crest (Samaan et al., 2010; Schmidt et al., 2011). Hex (also known as hhex) is expressed in migrating hepatic endoderm (Bogue et al., 2000), indirectly promotes migration of thyroid primordium (Parlato et al., 2004) and is also expressed mosaically in migrating anterior visceral endoderm (Srinivas et al., 2004). Foxo family TFs, particularly foxo1 and foxo3a, are well known as regulators of cell cycle arrest and apoptosis (Weidinger et al., 2008), but Foxo4 is also implicated in motility. Foxo4 is required for neural crest migration in *Xenopus laevis* and for *in vitro* smooth muscle cell migration (Schuff et al., 2010).

Thus, although motility is a less well-studied function for these three TFs, none is a surprising inclusion. Foxn2/3, hex and foxo do not have any regulatory inputs into one another, and therefore the motility sub-circuit functions via parallel inputs.

Apical constriction and AB polarity

The first visible morphological change that indicates an impending EMT is a thickened posterior epithelium caused by the elongation of the PMCs along their apical-basal axis. In control embryos, an apical constriction decreases the apical membrane diameter, creating an elongated cell in which much of the cytoplasm is forced basally. This requires actin-myosin contraction and properly maintained apical-basal polarity (Sawyer et al., 2010).

The shape change quantified in the present study suggested that apical constriction is controlled by a complex forward cascade that feeds into five terminal TFs: tel, hex, foxn2/3, foxb and foxo. Morphants depleted for these TFs and their upstream regulators are not able to make the characteristic long thin apical tail of controls, as shown by the principal component analysis. For each of these TFs, this is the first evidence of their involvement in apical constriction.

Interestingly, in *Drosophila* embryos, it is twist and snail that are thought to be responsible for apical constriction (Lye and Sanson, 2011). This may represent a protostome-specific function, as our present study shows that in the sea urchin (a deuterostome) snail and twist, along with their upstream regulator alx1, are not required for apical constriction. Additionally, we find no evidence in the current literature to suggest alx1, snail or twist regulate apical constriction in vertebrates. In fact, we were unable to find reports of transcription factors that regulate apical constriction in vertebrates. Many effector molecules of apical constriction (shroom, Rho, Rho kinase, myosin light chain kinase, enabled) are functionally conserved from invertebrates to vertebrates (Haigo et al., 2003; Sawyer et al., 2009; Bolinger et al., 2010), and these represent good candidates for future experiments to link the TFs in the apical constriction sub-circuit to downstream effector genes. However, it is not known how each of those effectors of apical constriction is transcriptionally regulated.

The de-adhesion sub-circuit involves snail and twist

Vertebrate development and cancer EMT models focus great attention on de-adhesion from the epithelium. The known drivers of vertebrate de-adhesion comprise seven TFs in three TF families: Snail (Snail1, Snail2 and Snail3), Twist (Twist1 and Twist2) and ZEB (ZEB1 and ZEB2). These TFs are all considered repressors of E-cadherin that promote de-adhesion (Sánchez-Tilló et al., 2012). The sea urchin genome did not go through whole genome duplications experienced by the vertebrate lineage, so each gene is present as a single copy (Sodergren et al., 2006). This makes study of snail and twist easier in our model, because in vertebrates the function(s) of snail (and others) could have been separated so that each snail gene may drive a different property.

Initially, it seemed the inclusion of alx1 in the de-adhesion sub-circuit was a sea urchin-specific function for this TF. In vertebrates, alx1 (also known as cart1) mutations have long been associated with craniofacial defects and neural tube defects without any known involvement in EMT (Zhao et al., 1996; Uz et al., 2010). However, recent vertebrate evidence shows a role for alx1 in EMT; in ovarian cancer cells, alx1 is reported to be upstream of snail-promoting EMT (Yuan et al., 2013). In the sea urchin de-adhesion sub-circuit, alx1 is upstream of both twist and snail, with twist also positively regulating alx1. This constitutes a positive feedback lock down mechanism for the regulation of de-adhesion.

We have previously reported a role for snail in sea urchin EMT (Wu and McClay, 2007). At that time, we observed that snail repressed cadherin transcriptionally. However, cadherin protein was abundant at the time of EMT and was endocytosed quickly and vanished at the end of EMT, presumably as a consequence of

lysosomal breakdown. These data suggested that snail repression of cadherin transcription was only part of the function of snail. Snail transcriptionally represses cadherin in virtually every animal model and cancer line where this was tested (Thiery et al., 2009), and recent evidence supports a role for Snail in the regulation of endocytosis in vertebrates (Kume et al., 2013). The snail-knockdown PMCs become even more elongated than the twist knockdown PMCs, but both knockdowns shared the property of failing to de-adhere. One possible explanation is that twist targets translational repression of cadherin, as it does in other organisms (Vesuna et al., 2008), but does not contribute to adherens junction demolition through endocytosis. It will be important to distinguish between those separate functions in future experiments.

Complexity of EMT regulation

In total, we discovered five PMC GRN sub-circuits that provide a first insight into the solution of the embryo for coordinating different cell state changes into one seemingly fluid morphogenetic movement of EMT (Fig. 7). The data support a model where unique sub-circuits of transcription factors regulate an embryonic EMT; each sub-circuit controls a distinct cell state change of the complex morphogenetic event. The sub-circuits themselves are unique but overlap, likely indicating that several TFs regulate effector genes essential to multiple cellular behaviors. The overlap of sub-circuits also provides a potential mechanism for coordinated timing and control of EMT. Each sub-circuit was a conservative call based on statistically significant differences from the mean control data, but even if other transcription factors were included in a sub-circuit, there was no case where a transcription factor could be included in all the sub-circuits.

To further test our observations, a cluster analysis of the total data set objectively grouped TFs together by EMT phenotype. That analysis supported individual sub-circuit model calls, and added confidence that the data accurately reflect distinct controls of cell behaviors in EMT. The resulting hierarchical tree (supplementary material Fig. S3) supplements the topological graphic of sub-circuits by showing the degree of TF relationships over a continuum of intermediate EMT phenotypes.

Cancer EMT has been studied far more extensively than developmental EMT, yet understanding the developmental mechanism is of crucial importance for cancer studies as evidence overwhelmingly suggests that cancer EMT is an aberrant deployment of the developmental EMT program (Thiery et al., 2009). In the chaotic cancer environment, the most infamous of the so-called EMT master regulators is snail (Wu and Zhou, 2010). Overexpression of snail in a cancer cell line is sufficient to induce EMT (Naber et al., 2013), yet overexpression in the embryo converts only a subpopulation of additional cells to an EMT state and not the entire embryo (Wu and McClay, 2007). These extra mesenchymal cells likely represent the precocious EMT of non-skeletogenic mesenchyme, a cell type already fated to undergo EMT later in development. Therefore, our data combined with previous study provide strong evidence that snail is not a master regulator of developmental EMT.

The complex sub-circuitry of the developmental EMT provides an alternate hypothesis for how overexpression of TFs such as snail and twist can ectopically induce the full EMT program. In the Lv PMC GRN, snail regulates erg and erg regulates hex; overstimulation of this regulatory pathway through snail expression could easily activate four out of the five sub-circuits. Without the context of the GRN and its sub-circuitry, it is easy to see how snail could be misinterpreted as inducing EMT alone.

Knowledge of these distinct sub-circuits underscores the importance of interpreting EMT activity of transcription factors within the context of a regulatory network. The sub-circuits also provide new tools for future detailed analysis of each EMT cell state change and their corresponding terminal effector genes. Thus, the discovery of these sub-circuits redefines the transcriptional control of EMT and highlights the complex, cooperative regulation underlying this morphogenetic movement, which is of significance to development, regenerative medicine and cancer biology.

MATERIALS AND METHODS

Animals

Sexually mature *Lytechinus variegatus* adult sea urchins were obtained from Reeftopia (Key West, FL, USA), Sea Life (Tavernier, FL, USA) or the Duke University Marine Lab (Beaufort, NC, USA). Gametes were collected by coelomic injection of 0.5 M KCl. Embryos were cultured at 23°C in artificial seawater (ASW).

Cloning Lv PMC transcription factors

Primer sets were designed to annotated *S. purpuratus* coding sequences for cloning the following transcription factors in *L. variegatus*, LvDri, LvErg, LvFoxB, LvFoxO, LvHex, LvTel and LvTgif, that had not been cloned previously in this species. When the *L. variegatus* genome assembly became available in 2011, the sequence of all seven cloned transcription factor sequences matched the genome sequences. See supplementary material Table S1 for primer oligo sequences.

Transcription factor knockdowns and fluorescent markers

Two non-overlapping morpholino antisense oligonucleotides (MASOs) targeted to each one of the seven cloned PMC transcription factors were designed and synthesized by Gene Tools. The effective concentrations were determined: 2.0 mM LvDri1, 1.5 mM LvDri2, 0.75 mM LvErg1, 0.5 mM LvErg2, 0.3 mM LvFoxB1, 0.5 mM LvFoxB2, 1.0 mM LvFoxO1, 0.75 mM LvFoxO2, 2.0 mM LvHex1, 1.5 mM LvHex2, 0.75 mM LvTel1, 1.0 mM LvTel2, 0.5 mM LvTgif1 and 1.0 mM LvTgif2. Each pair of morpholino knockdowns to the seven transcription factors had a phenotype uniquely seen for that pair. See supplementary material Table S2 for MASO oligo sequences. The following concentrations were used for previously published Lv PMC transcription factor MASOs used in this study: 1.0 mM LvAlx1 (Ettensohn et al., 2003), 1.0 mM LvSnail2 (Wu and McClay, 2007), 1.5 mM LvTwist (Wu et al., 2008), 0.5 mM LvTbr (Croce et al., 2001) and 0.7 mM FoxN2/3-1 (Rho and McClay, 2011). mRNA for injection was transcribed *in vitro* using Ambion mMessage mMachine. Concentrations for mRNA injections: 750 ng/µl dominant-negative LvEts1 (DNEts1) (Sharma and Ettensohn, 2010), 250 ng/µl Histone2B-GFP (H2B-GFP), 500 ng/µl H2B-RFP, 750 ng/µl membrane-RFP (mem-RFP) and 500 ng/µl mem-GFP.

Injections and microsurgery

Fertilized embryos were triple injected with either mem-GFP and H2B-RFP or mem-RFP and H2B-GFP, and either 0.5 mM of standard control MASO or a knockdown directed towards one of the transcription factors. At 2.5 hpf, micromeres were transplanted; one micromere from an injected donor embryo was inserted onto an uninjected 16-cell host embryo from the same parental cross in the place of one discarded host micromere. Detailed methods of injections and transplants were followed as previously described (Logan et al., 1999; Sherwood and McClay, 1999).

Live image acquisition

At 8.5 hpf, embryos were de-ciliated in 2× hypertonic artificial seawater, mounted in 1× artificial seawater containing 10 µM p-methoxy-phenyl isoxazoline (Semenova et al., 2008) on a slide coated in 2% protamine sulfate and sealed with V.A.L.A.P. Images were acquired using Coolsnap high-resolution CCD camera on either the Zeiss Axio Observer Z1 with 63×/1.4 Oil Plan-Apochromat DIC objective or the DeltaVision Elite with 40×/0.65-1.35 Oil UAPO40X0I3/340 DIC objective. Images were collected at 60-second intervals beginning at 9.0 hpf and ending at 12.0 hpf or later,

and projected as movies using Metamorph for Zeiss data or SoftWorx for DeltaVision data.

Principal component analysis

Cell membranes were manually segmented using Adobe Photoshop CS5.1 and analyzed using SHAPE ver. 1.3 (Iwata and Ukai, 2002). Outlines were elliptical Fourier transformed to the first 20 harmonics; transforms were normalized along the apical-basal axis of each cell and principal component analysis was performed (Kuhl and Giardina, 1982; Iwata et al., 2004).

Motility analysis

Time-lapse movies were registered and fluorescent cell area was measured using FIJI (Schindelin et al., 2012). The membrane channel was made binary, nuclei were marked with Find Maxima and each was measured using the Analyze Particles tool. The basement membrane (BM) boundary in the DIC reference was manually segmented. Inside the boundary (the blastocoel) was deleted for corresponding fluorescent images for both channels and were measured using Analyze Particles. Measurements with blastocoel removed were divided by original measurements to find the percentage of GFP cell area and percentage of nuclei within the epithelium.

Immunostaining and fixed imaging

Embryos were fixed at 10 hpf and double immunostained with monoclonal 1D5 antibody (1:1) and polyclonal anti-laminin antibody (1:300) (Abcam, ab11575), and subsequently stained with Hoechst's (1:1000) (Molecular Probes). Fixative used was 100% methanol. Images were acquired using Zeiss LSM 510 upright confocal with a 40×/1.4 Oil Plan-Apochromat objective. *Z*-slices were spaced 1.0 µm or 0.5 µm apart spanning the diameter of the embryo.

Image processing and statistical analysis of immunostains

Three-dimensional projections of control embryos were rendered from confocal *z*-slices spaced 0.5 µm apart using Imaris v.7.1.1 (Bitplane). Two-dimensional projections were rendered in Fiji from *z*-slice = N/2 + 5 through *z*-slice = N/2 – 5, where N is the sum of *z*-slices, for slices spaced 1.0 µm apart for a 10 µm projection through the center of the embryo. Projections were rotated with thickened posterior and/or apical nuclei to bottom center. Images were cropped to bound nuclei and pixel intensity values were measured using Fiji > Analyze > Measure > Raw Int Density as defined by a rectangular section Rectangle = (*x*, *y*, width, height), for three rectangular selections with scale set to µm: Lateral Left Rectangle = (0, (height/2 – 5), width/2, 10); Lateral Right Rectangle = (width/2, (height/2 – 5), width/2, 10); and Center Vegetal Rectangle = ((width/2 – 5), height/2, 10, height/2).

Cluster analysis

Phenotype data were clustered using CLUTO v.2.1.2 (Karypis, 2002) under the parameters [CLMethod=RBR, CRfun=I2, SimFun=CorrCoef, #Clusters: 6]. The similarity function chosen provided the widest variance in resulting clusters. Laminin hole measurements were weighted 0.25 to compare with continuous motility and shape measurements.

Acknowledgements

We thank M. Semenova for providing reagents and S. Johnson for microscopy support. We thank D. Kiehart, X. Dong, G. Wray, F. Nijhout, D. Sherwood, J. P. Thiery and members of the McClay lab for critical discussion of experiments and results.

Competing interests

The authors declare no competing financial interests.

Author contributions

L.R.S. performed experiments, carried out the statistical tests and wrote the manuscript. D.R.M. performed experiments, wrote and edited the manuscript.

Funding

This work was supported by grants from the National Institutes of Health (NIH) [HD 14483, HD 037105 and GM 081883]. Deposited in PMC for release after 12 months.

Supplementary material

Supplementary material available online at
http://dev.biologists.org/lookup/suppl/doi:10.1242/dev.101436/-/DC1

References

Acloque, H., Adams, M. S., Fishwick, K., Bronner-Fraser, M. and Nieto, M. A. (2009). Epithelial-mesenchymal transitions: the importance of changing cell state in development and disease. *J. Clin. Invest.* **119**, 1438-1449.

Anderson, K. V. and Nusslein-Volhard, C. (1984). *Genetic Analysis of Dorsoventral Embryonic Pattern in Drosophila*, pp. 10-20. New York, NY: MacMillan.

Angerer, L., Hussain, S., Wei, Z. and Livingston, B. T. (2006). Sea urchin metalloproteases: a genomic survey of the BMP-1/tolloid-like, MMP and ADAM families. *Dev. Biol.* **300**, 267-281.

Baillat, D., Leprivier, G., Régnier, D., Vintonenko, N., Bègue, A., Stéhelin, D. and Aumercier, M. (2006). Stromelysin-1 expression is activated in vivo by Ets-1 through palindromic head-to-head Ets binding sites present in the promoter. *Oncogene* **25**, 5764-5776.

Batlle, E., Sancho, E., Francí, C., Domínguez, D., Monfar, M., Baulida, J. and García De Herreros, A. (2000). The transcription factor snail is a repressor of E-cadherin gene expression in epithelial tumour cells. *Nat. Cell Biol.* **2**, 84-89.

Benson, S., Page, L., Ingersoll, E., Rosenthal, E., Dungca, K. and Signor, D. (1999). Developmental characterization of the gene for laminin alpha-chain in sea urchin embryos. *Mech. Dev.* **81**, 37-49.

Bertolino, E., Wildt, S., Richards, G. and Clerc, R. G. (1996). Expression of a novel murine homeobox gene in the developing cerebellar external granular layer during its proliferation. *Dev. Dyn.* **205**, 410-420.

Bogue, C. W., Ganea, G. R., Sturm, E., Ianucci, R. and Jacobs, H. C. (2000). Hex expression suggests a role in the development and function of organs derived from foregut endoderm. *Dev. Dyn.* **219**, 84-89.

Bolinger, C., Zasadil, L., Rizaldy, R. and Hildebrand, J. D. (2010). Specific isoforms of drosophila shroom define spatial requirements for the induction of apical constriction. *Dev. Dyn.* **239**, 2078-2093.

Bradley, C. K., Norton, C. R., Chen, Y., Han, X., Booth, C. J., Yoon, J. K., Krebs, L. T. and Gridley, T. (2013). The snail family gene snai3 is not essential for embryogenesis in mice. *PLoS ONE* **8**, e65344.

Cano, A., Pérez-Moreno, M. A., Rodrigo, I., Locascio, A., Blanco, M. J., del Barrio, M. G., Portillo, F. and Nieto, M. A. (2000). The transcription factor snail controls epithelial-mesenchymal transitions by repressing E-cadherin expression. *Nat. Cell Biol.* **2**, 76-83.

Chen, Q. K., Lee, K., Radisky, D. C. and Nelson, C. M. (2013). Extracellular matrix proteins regulate epithelial-mesenchymal transition in mammary epithelial cells. *Differentiation* **86**, 126-132.

Croce, J., Lhomond, G., Lozano, J. C. and Gache, C. (2001). ske-T, a T-box gene expressed in the skeletogenic mesenchyme lineage of the sea urchin embryo. *Mech. Dev.* **107**, 159-162.

D'Souza-Schorey, C. (2005). Disassembling adherens junctions: breaking up is hard to do. *Trends Cell Biol.* **15**, 19-26.

Davidson, E. H., Rast, J. P., Oliveri, P., Ransick, A., Calestani, C., Yuh, C. H., Minokawa, T., Amore, G., Hinman, V., Arenas-Mena, C. et al. (2002). A genomic regulatory network for development. *Science* **295**, 1669-1678.

Davidson, E. H. (2006). The sea urchin genome: where will it lead us? *Science* **314**, 939-940.

Ettensohn, C. A. (1990). Cell interactions in the sea urchin embryo studied by fluorescence photoablation. *Science* **248**, 1115-1118.

Ettensohn, C. A., Illies, M. R., Oliveri, P. and De Jong, D. L. (2003). Alx1, a member of the Cart1/Alx3/Alx4 subfamily of Paired-class homeodomain proteins, is an essential component of the gene network controlling skeletogenic fate specification in the sea urchin embryo. *Development* **130**, 2917-2928.

Ghosh, S., Basu, M. and Roy, S. S. (2012). ETS-1 protein regulates vascular endothelial growth factor-induced matrix metalloproteinase-9 and matrix metalloproteinase-13 expression in human ovarian carcinoma cell line SKOV-3. *J. Biol. Chem.* **287**, 15001-15015.

Haigo, S. L., Hildebrand, J. D., Harland, R. M. and Wallingford, J. B. (2003). Shroom induces apical constriction and is required for hingepoint formation during neural tube closure. *Curr. Biol.* **13**, 2125-2137.

Hopwood, N. D., Pluck, A. and Gurdon, J. B. (1989). A Xenopus mRNA related to Drosophila twist is expressed in response to induction in the mesoderm and the neural crest. *Cell* **59**, 893-903.

Iwata, H. and Ukai, Y. (2002). SHAPE: a computer program package for quantitative evaluation of biological shapes based on elliptic Fourier descriptors. *J. Hered.* **93**, 384-385.

Iwata, H., Niikura, S., Matsuura, S., Takano, Y. and Ukai, Y. (2004). Interaction between genetic effects and soil type in diallel analysis of root shape and size of Japanese radish (Raphanus sativus L.). *Breed. Sci.* **54**, 313-318.

Jin, L., Zhou, Y., Kuang, C., Lin, L. and Chen, Y. (2005). Expression pattern of TG-interacting factor 2 during mouse development. *Gene Expr. Patterns* **5**, 457-462.

Kalluri, R. and Weinberg, R. A. (2009). The basics of epithelial-mesenchymal transition. *J. Clin. Invest.* **119**, 1420-1428.

Karypis, G. (2002). *CLUTO a Clustering Toolkit.* Minneapolis, MN: Department of Computer Science, University of Minnesota.

Kataoka, H., Murayama, T., Yokode, M., Mori, S., Sano, H., Ozaki, H., Yokota, Y., Nishikawa, S. and Kita, T. (2000). A novel snail-related transcription factor Smuc regulates basic helix-loop-helix transcription factor activities via specific E-box motifs. *Nucleic Acids Res.* **28**, 626-633.

Kim, A., Kim, E. Y., Cho, E. N., Kim, H. J., Kim, S. K., Chang, J., Ahn, C. M. and Chang, Y. S. (2013). Notch1 destabilizes the adherens junction complex through upregulation of the Snail family of E-cadherin repressors in non-small cell lung cancer. *Oncol. Rep.* **30**, 1423-1429.
Kuhl, F. P. and Giardina, C. R. (1982). Elliptic Fourier features of a closed contour. *Computer Graphics and Image Processing* **18**, 236-258.
Kume, K., Haraguchi, M., Hijioka, H., Ishida, T., Miyawaki, A., Nakamura, N. and Ozawa, M. (2013). The transcription factor Snail enhanced the degradation of E-cadherin and desmoglein 2 in oral squamous cell carcinoma cells. *Biochem. Biophys. Res. Commun.* **430**, 889-894.
Lee, T. K., Poon, R. T., Yuen, A. P., Ling, M. T., Kwok, W. K., Wang, X. H., Wong, Y. C., Guan, X. Y., Man, K., Chau, K. L. et al. (2006). Twist overexpression correlates with hepatocellular carcinoma metastasis through induction of epithelial-mesenchymal transition. *Clin. Cancer Res.* **12**, 5369-5376.
Levayer, R. and Lecuit, T. (2008). Breaking down EMT. *Nat. Cell Biol.* **10**, 757-759.
Logan, C. Y., Miller, J. R., Ferkowicz, M. J. and McClay, D. R. (1999). Nuclear beta-catenin is required to specify vegetal cell fates in the sea urchin embryo. *Development* **126**, 345-357.
Lye, C. M. and Sanson, B. (2011). Tension and epithelial morphogenesis in Drosophila early embryos. *Curr. Top. Dev. Biol.* **95**, 145-187.
Moustakas, A. and Heldin, C. H. (2012). Induction of epithelial-mesenchymal transition by transforming growth factor β. *Semin. Cancer Biol.* **22**, 446-454.
Naber, H. P., Drabsch, Y., Snaar-Jagalska, B. E., ten Dijke, P. and van Laar, T. (2013). Snail and Slug, key regulators of TGF-β-induced EMT, are sufficient for the induction of single-cell invasion. *Biochem. Biophys. Res. Commun.* **435**, 58-63.
Oda, H., Tsukita, S. and Takeichi, M. (1998). Dynamic behavior of the cadherin-based cell-cell adhesion system during Drosophila gastrulation. *Dev. Biol.* **203**, 435-450.
Oliveri, P., Tu, Q. and Davidson, E. H. (2008). Global regulatory logic for specification of an embryonic cell lineage. *Proc. Natl. Acad. Sci. U.S.A.* **105**, 5955-5962.
Parlato, R., Rosica, A., Rodriguez-Mallon, A., Affuso, A., Postiglione, M. P., Arra, C., Mansouri, A., Kimura, S., Di Lauro, R. and De Felice, M. (2004). An integrated regulatory network controlling survival and migration in thyroid organogenesis. *Dev. Biol.* **276**, 464-475.
Powers, S. E., Taniguchi, K., Yen, W., Melhuish, T. A., Shen, J., Walsh, C. A., Sutherland, A. E. and Wotton, D. (2010). Tgif1 and Tgif2 regulate Nodal signaling and are required for gastrulation. *Development* **137**, 249-259.
Rafiq, K., Cheers, M. S. and Ettensohn, C. A. (2012). The genomic regulatory control of skeletal morphogenesis in the sea urchin. *Development* **139**, 579-590.
Rho, H. K. and McClay, D. R. (2011). The control of foxN2/3 expression in sea urchin embryos and its function in the skeletogenic gene regulatory network. *Development* **138**, 937-945.
Rowe, R. G. and Weiss, S. J. (2008). Breaching the basement membrane: who, when and how? *Trends Cell Biol.* **18**, 560-574.
Samaan, G., Yugo, D., Rajagopalan, S., Wall, J., Donnell, R., Goldowitz, D., Gopalakrishnan, R. and Venkatachalam, S. (2010). Foxn3 is essential for craniofacial development in mice and a putative candidate involved in human congenital craniofacial defects. *Biochem. Biophys. Res. Commun.* **400**, 60-65.
Sánchez-Tilló, E., Liu, Y., de Barrios, O., Siles, L., Fanlo, L., Cuatrecasas, M., Darling, D. S., Dean, D. C., Castells, A. and Postigo, A. (2012). EMT-activating transcription factors in cancer: beyond EMT and tumor invasiveness. *Cell. Mol. Life Sci.* **69**, 3429-3456.
Sargent, M. G. and Bennett, M. F. (1990). Identification in Xenopus of a structural homologue of the Drosophila gene snail. *Development* **109**, 967-973.
Sawyer, J. K., Harris, N. J., Slep, K. C., Gaul, U. and Peifer, M. (2009). The Drosophila afadin homologue Canoe regulates linkage of the actin cytoskeleton to adherens junctions during apical constriction. *J. Cell Biol.* **186**, 57-73.
Sawyer, J. M., Harrell, J. R., Shemer, G., Sullivan-Brown, J., Roh-Johnson, M. and Goldstein, B. (2010). Apical constriction: a cell shape change that can drive morphogenesis. *Dev. Biol.* **341**, 5-19.
Schindelin, J., Arganda-Carreras, I., Frise, E., Kaynig, V., Longair, M., Pietzsch, T., Preibisch, S., Rueden, C., Saalfeld, S., Schmid, B. et al. (2012). Fiji: an open-source platform for biological-image analysis. *Nat. Methods* **9**, 676-682.
Schmidt, J., Schuff, M. and Olsson, L. (2011). A role for FoxN3 in the development of cranial cartilages and muscles in Xenopus laevis (Amphibia: Anura: Pipidae) with special emphasis on the novel rostral cartilages. *J. Anat.* **218**, 226-242.
Schuff, M., Siegel, D., Bardine, N., Oswald, F., Donow, C. and Knöchel, W. (2010). FoxO genes are dispensable during gastrulation but required for late embryogenesis in Xenopus laevis. *Dev. Biol.* **337**, 259-273.
Semenova, M. N., Tsyganov, D. V., Yakubov, A. P., Kiselyov, A. S. and Semenov, V. V. (2008). A synthetic derivative of plant allylpolyalkoxybenzenes induces selective loss of motile cilia in sea urchin embryos. *ACS Chem. Biol.* **3**, 95-100.
Sharma, T. and Ettensohn, C. A. (2010). Activation of the skeletogenic gene regulatory network in the early sea urchin embryo. *Development* **137**, 1149-1157.
Shen, J. and Walsh, C. A. (2005). Targeted disruption of Tgif, the mouse ortholog of a human holoprosencephaly gene, does not result in holoprosencephaly in mice. *Mol. Cell. Biol.* **25**, 3639-3647.
Sherwood, D. R. and McClay, D. R. (1999). LvNotch signaling mediates secondary mesenchyme specification in the sea urchin embryo. *Development* **126**, 1703-1713.
Shook, D. and Keller, R. (2003). Mechanisms, mechanics and function of epithelial-mesenchymal transitions in early development. *Mech. Dev.* **120**, 1351-1383.
Siletz, A., Schnabel, M., Kniazeva, E., Schumacher, A. J., Shin, S., Jeruss, J. S. and Shea, L. D. (2013). Dynamic transcription factor networks in epithelial-mesenchymal transition in breast cancer models. *PLoS ONE* **8**, e57180.
Simpson, P. (1983). Maternal-zygotic gene interactions during formation of the dorsoventral pattern in drosophila embryos. *Genetics* **105**, 615-632.
Sodergren, E., Weinstock, G. M., Davidson, E. H., Cameron, R. A., Gibbs, R. A., Angerer, R. C., Angerer, L. M., Arnone, M. I., Burgess, D. R., Burke, R. D. et al.; Sea Urchin Genome Sequencing Consortium (2006). The genome of the sea urchin Strongylocentrotus purpuratus. *Science* **314**, 941-952.
Srinivas, S., Rodriguez, T., Clements, M., Smith, J. C. and Beddington, R. S. (2004). Active cell migration drives the unilateral movements of the anterior visceral endoderm. *Development* **131**, 1157-1164.
Thiery, J. P., Acloque, H., Huang, R. Y. and Nieto, M. A. (2009). Epithelial-mesenchymal transitions in development and disease. *Cell* **139**, 871-890.
Turbeville, J. M., Schulz, J. R. and Raff, R. A. (1994). Deuterostome phylogeny and the sister group of the chordates: evidence from molecules and morphology. *Mol. Biol. Evol.* **11**, 648-655.
Uz, E., Alanay, Y., Aktas, D., Vargel, I., Gucer, S., Tuncbilek, G., von Eggeling, F., Yilmaz, E., Deren, O., Posorski, N. et al. (2010). Disruption of ALX1 causes extreme microphthalmia and severe facial clefting: expanding the spectrum of autosomal-recessive ALX-related frontonasal dysplasia. *Am. J. Hum. Genet.* **86**, 789-796.
Vesuna, F., van Diest, P., Chen, J. H. and Raman, V. (2008). Twist is a transcriptional repressor of E-cadherin gene expression in breast cancer. *Biochem. Biophys. Res. Commun.* **367**, 235-241.
Weidinger, C., Krause, K., Klagge, A., Karger, S. and Fuhrer, D. (2008). Forkhead box-O transcription factor: critical conductors of cancer's fate. *Endocr. Relat. Cancer* **15**, 917-929.
Westermarck, J., Seth, A. and Kähäri, V. M. (1997). Differential regulation of interstitial collagenase (MMP-1) gene expression by ETS transcription factors. *Oncogene* **14**, 2651-2660.
Wu, Y. and Zhou, B. P. (2010). Snail: more than EMT. *Cell Adh. Migr.* **4**, 199-203.
Wu, S. Y. and McClay, D. R. (2007). The Snail repressor is required for PMC ingression in the sea urchin embryo. *Development* **134**, 1061-1070.
Wu, S. Y., Yang, Y. P. and McClay, D. R. (2008). Twist is an essential regulator of the skeletogenic gene regulatory network in the sea urchin embryo. *Dev. Biol.* **319**, 406-415.
Yang, J. and Weinberg, R. A. (2008). Epithelial-mesenchymal transition: at the crossroads of development and tumor metastasis. *Dev. Cell* **14**, 818-829.
Yap, A. S., Crampton, M. S. and Hardin, J. (2007). Making and breaking contacts: the cellular biology of cadherin regulation. *Curr. Opin. Cell Biol.* **19**, 508-514.
Yuan, H., Kajiyama, H., Ito, S., Yoshikawa, N., Hyodo, T., Asano, E., Hasegawa, H., Maeda, M., Shibata, K., Hamaguchi, M. et al. (2013). ALX1 induces snail expression to promote epithelial-to-mesenchymal transition and invasion of ovarian cancer cells. *Cancer Res.* **73**, 1581-1590.
Zhao, Q., Behringer, R. R. and de Crombrugghe, B. (1996). Prenatal folic acid treatment suppresses acrania and meroanencephaly in mice mutant for the Cart1 homeobox gene. *Nat. Genet.* **13**, 275-283.
Zheng, H. and Kang, Y. (2013). Multilayer control of the EMT master regulators. *Oncogene* doi:10.1038/onc.2013.128 (in press).

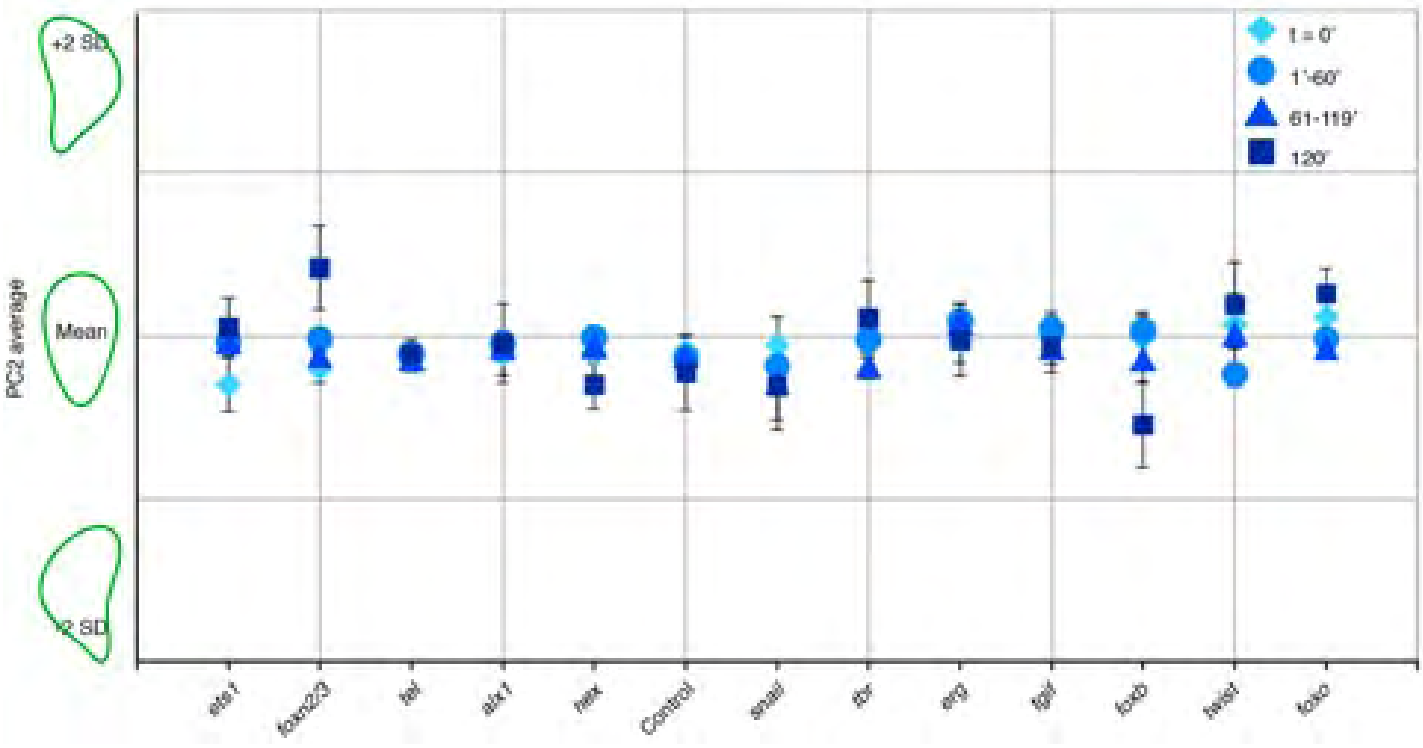

Fig. S1. PC2 represents lateral asymmetry of cell shape. PC2 does not show significant variation over elapsed time or between TF knockdowns. Time (t) is in minutes. Error bars are s.e.m.

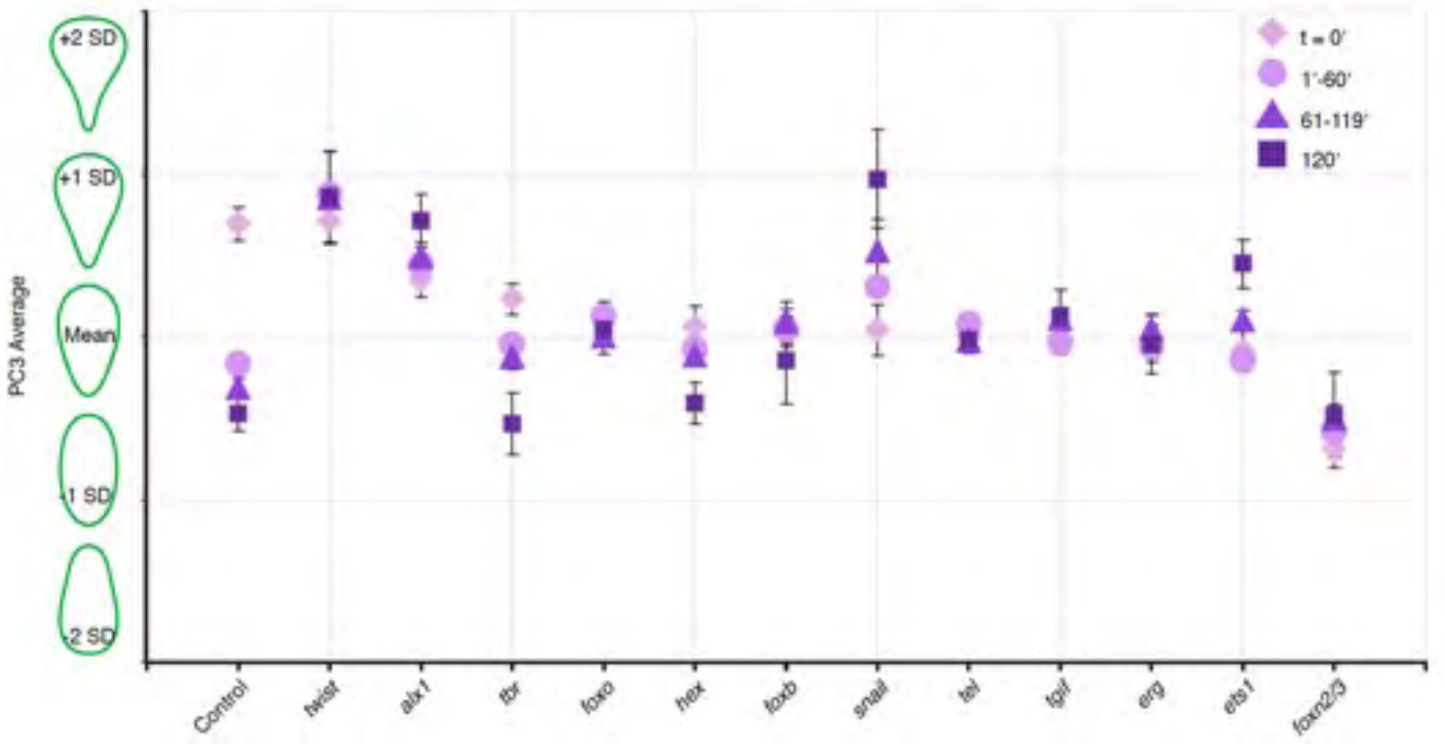

Fig. S2. Foxn2/3 and tbr are required for apical-basal polarity. PC3 represents cytoplasm distribution along the apical-basal axis from polarized apically, −2 SD, to polarized basally with minor apical constriction, +2 s.d. Foxn2/3 is the only knockdown to average more apical cytoplasm than the mean shape across all time points and tbr has progressively more apical cytoplasm over the time-course. Time is in minutes.

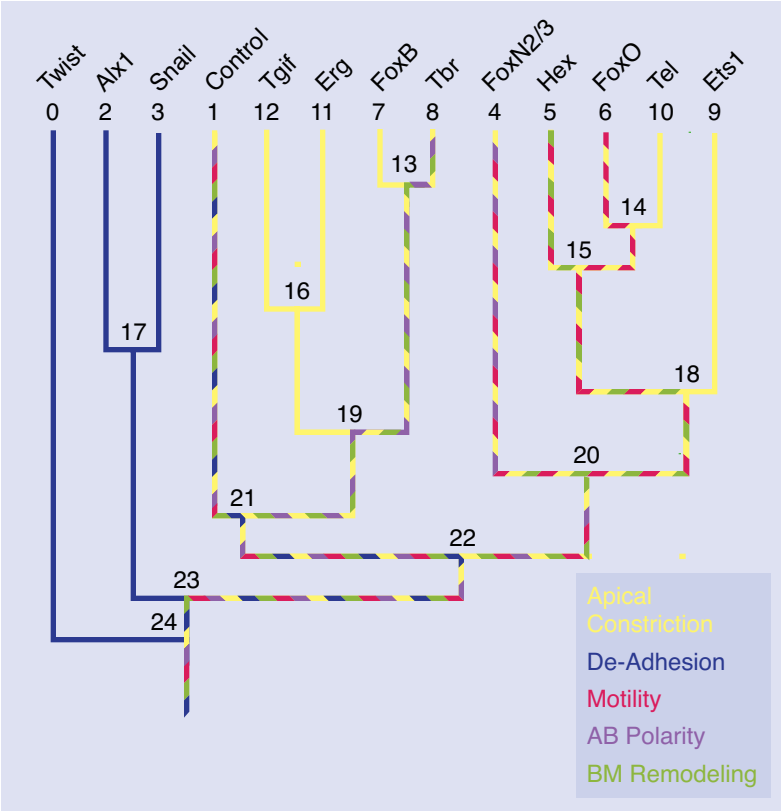

Fig. S3. Unsupervised analysis of TF knockdown phenotypes. K-means cluster analysis of displacement, principal component, and BM remodeling data. The hierarchical tree resulting from clustering shows the relationships between TFs based on total phenotypes. Five cellular behaviors of EMT are color coded; apical constriction (yellow), motility (red), apical-basal (AB) polarity (purple), de-adhesion (blue), and BM remodeling (green).

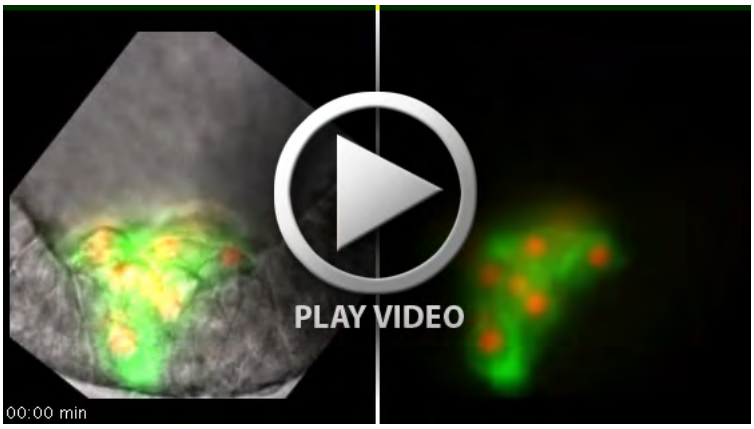

Movie 1. Time-lapse of Control-1. Green label is cell membrane (mem-GFP). Red label is nuclei (H2B-RFP). Left panel: DIC, mem-GFP, H2B-RFP. Right panel: mem-GFP, H2B-RFP.

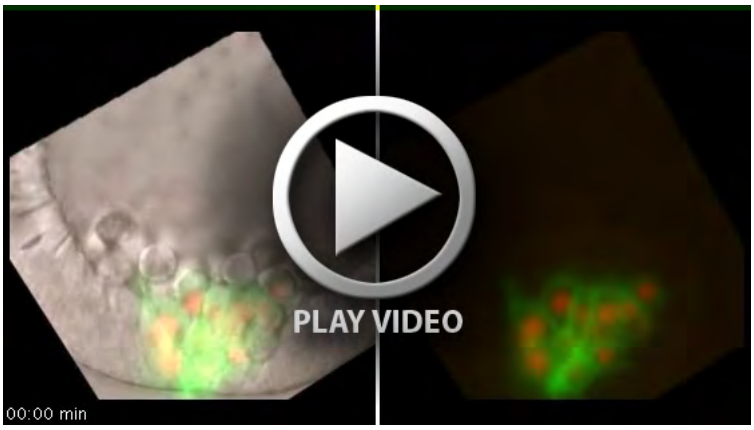

Movie 2. Time-lapse of Control-2. Green label is cell membrane (mem-GFP). Red label is nuclei (H2B-RFP). Left panel: DIC, mem-GFP, H2B-RFP. Right panel: mem-GFP, H2B-RFP.

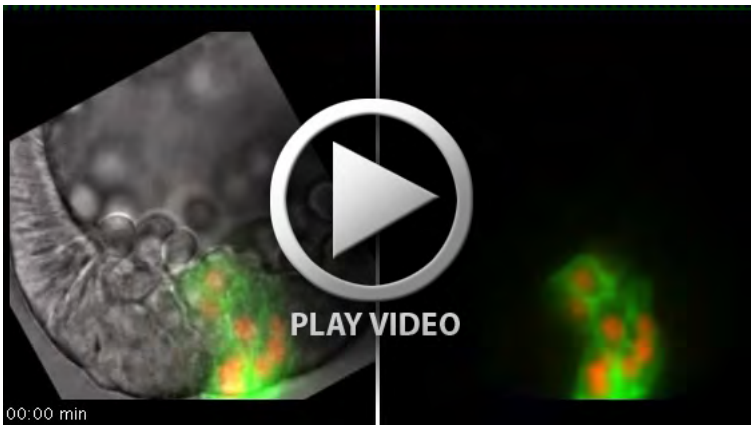

Movie 3. Time-lapse of alx1 morpholino antisense oligonucleotide knockdown. Green label is cell membrane (mem-GFP). Red label is nuclei (H2B-RFP). Left panel: DIC, mem-GFP, H2B-RFP. Right panel: mem-GFP, H2B-RFP.

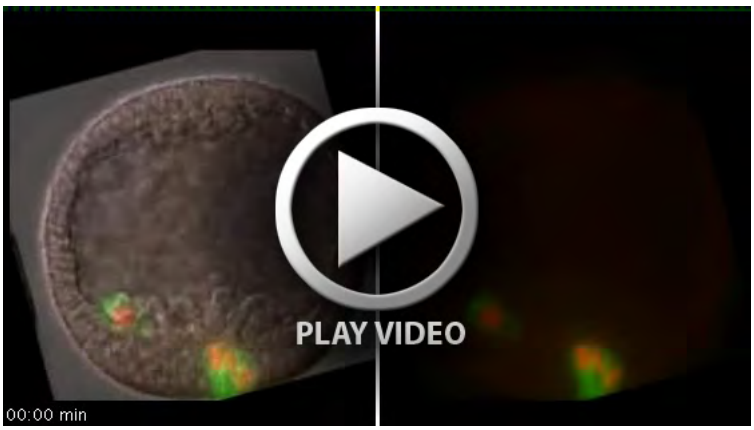

Movie 4. Time-lapse of erg morpholino antisense oligonucleotide knockdown. Green label is cell membrane (mem-GFP). Red label is nuclei (H2B-RFP). Left panel: DIC, mem-GFP, H2B-RFP. Right panel: mem-GFP, H2B-RFP.

Movie 5. Time-lapse of ets1 dominant-negative knockdown. Green label is cell membrane (mem-GFP). Red label is nuclei (H2B-RFP). Left panel: DIC, mem-GFP, H2B-RFP. Right panel: mem-GFP, H2B-RFP.

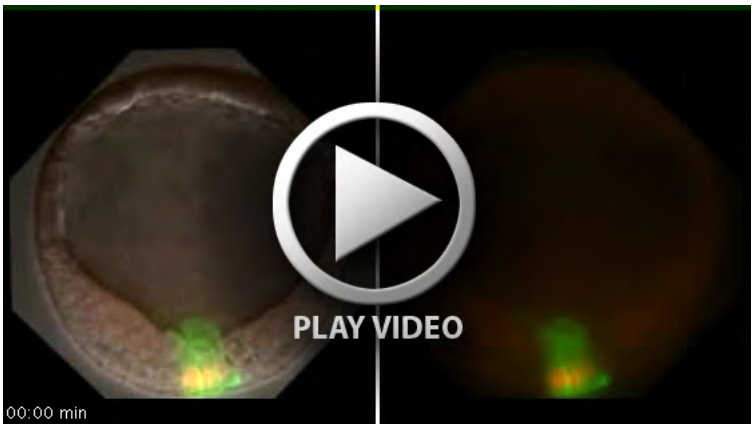

Movie 6. Time-lapse of foxb morpholino antisense oligonucleotide knockdown. Green label is cell membrane (mem-GFP). Red label is nuclei (H2B-RFP). Left panel: DIC, mem-GFP, H2B-RFP. Right panel: mem-GFP, H2B-RFP.

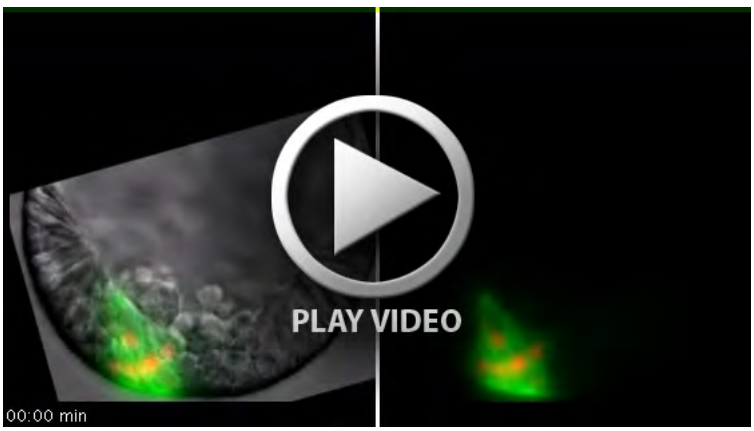

Movie 7. Time-lapse of foxn2/3 morpholino antisense oligonucleotide knockdown. Green label is cell membrane (mem-GFP). Red label is nuclei (H2B-RFP). Left panel: DIC, mem-GFP, H2B-RFP. Right panel: mem-GFP, H2B-RFP.

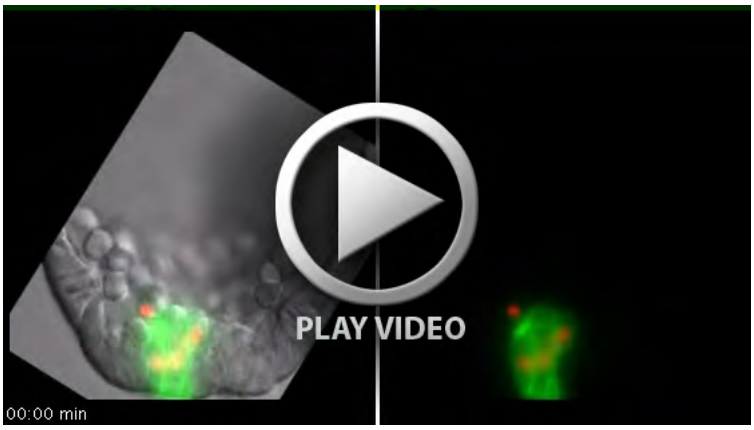

Movie 8. Time-lapse of foxo morpholino antisense oligonucleotide knockdown. Green label is cell membrane (mem-GFP). Red label is nuclei (H2B-RFP). Left panel: DIC, mem-GFP, H2B-RFP. Right panel: mem-GFP, H2B-RFP.

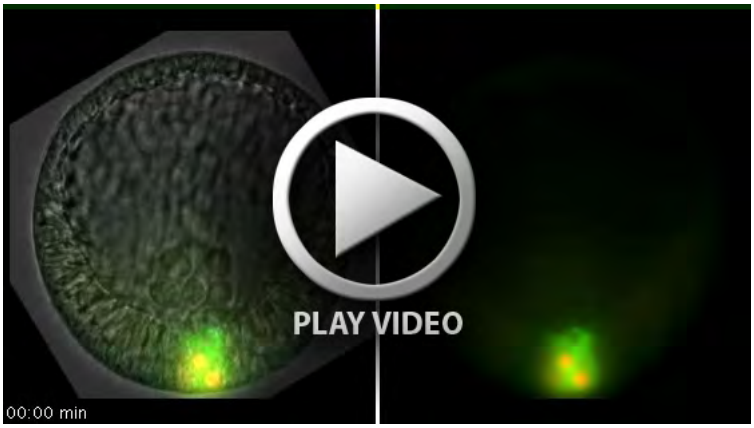

Movie 9. Time-lapse of hex morpholino antisense oligonucleotide knockdown. Green label is cell membrane (mem-GFP). Red label is nuclei (H2B-RFP). Left panel: DIC, mem-GFP, H2B-RFP. Right panel: mem-GFP, H2B-RFP.

Movie 10. Time-lapse of snail morpholino antisense oligonucleotide knockdown. Green label is cell membrane (mem-GFP). Red label is nuclei (H2B-RFP). Left panel: DIC, mem-GFP, H2B-RFP. Right panel: mem-GFP, H2B-RFP.

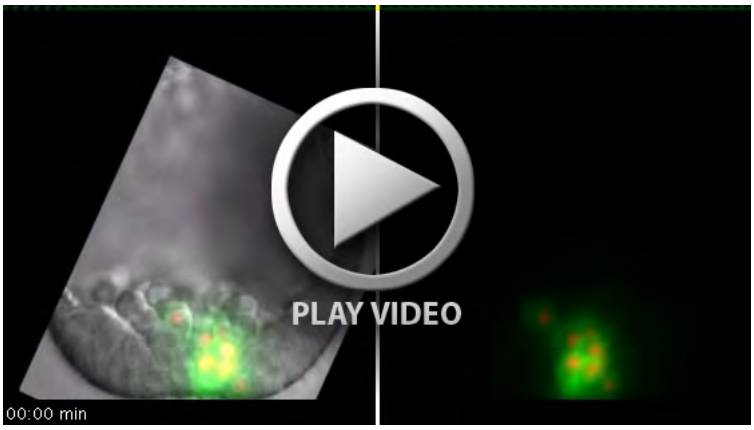

Movie 11. Time-lapse of tbr morpholino antisense oligonucleotide knockdown. Green label is cell membrane (mem-GFP). Red label is nuclei (H2B-RFP). Left panel: DIC, mem-GFP, H2B-RFP. Right panel: mem-GFP, H2B-RFP.

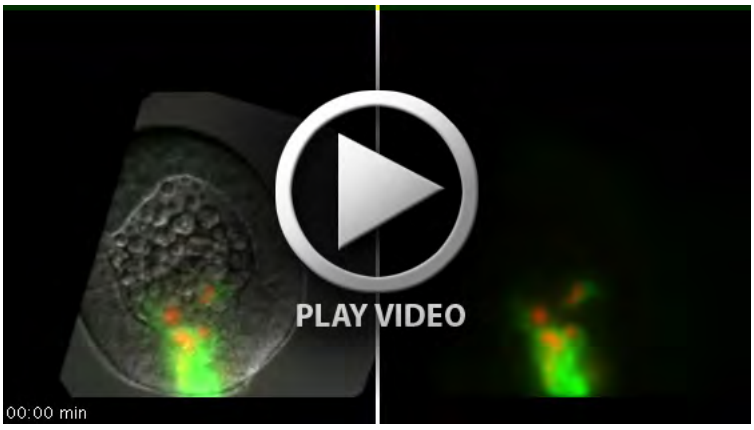

Movie 12. Time-lapse of tel morpholino antisense oligonucleotide knockdown. Green label is cell membrane (mem-GFP). Red label is nuclei (H2B-RFP). Left panel: DIC, mem-GFP, H2B-RFP. Right panel: mem-GFP, H2B-RFP.

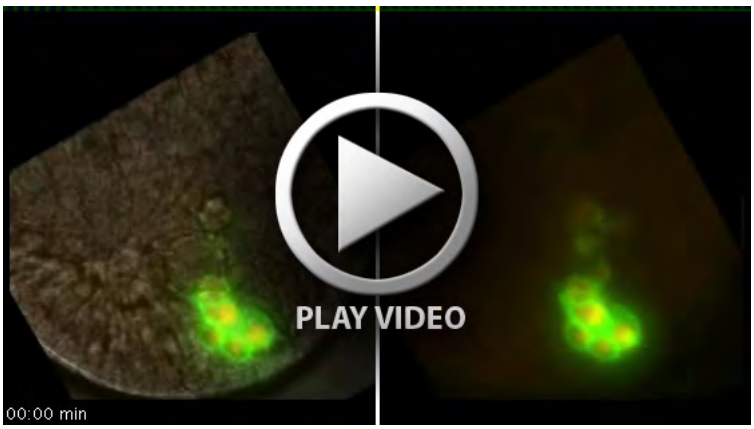

Movie 13. Time-lapse of tgif morpholino antisense oligonucleotide knockdown. Green label is cell membrane (mem-GFP). Red label is nuclei (H2B-RFP). Left panel: DIC, mem-GFP, H2B-RFP. Right panel: mem-GFP, H2B-RFP.

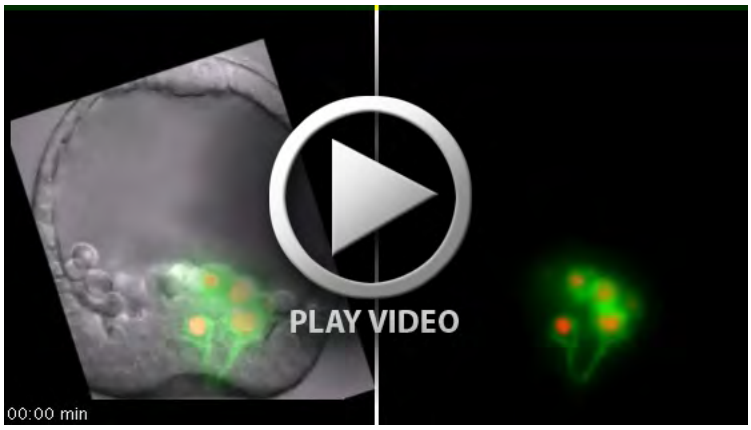

Movie 14. Time-lapse of twist morpholino antisense oligonucleotide knockdown. Green label is cell membrane (mem-GFP). Red label is nuclei (H2B-RFP). Left panel: DIC, mem-GFP, H2B-RFP. Right panel: mem-GFP, H2B-RFP.

Table S1. Primer Sequences

Gene	Forward Primer	Reverse Primer
Dri	5’ – GTAACACTGACTTTAGCGATCCTTCG – 3’	5’ – GCTCAGATGGTGAACTCAAACTCTTC – 3’
Erg	5’ – TCCGACTGCCTTTTGAGT AAAGCAACGTCG – 3’	5’ – GCACTTCGTTTACGAGTCT TTGTAATAGGAGTCC – 3’
FoxB	5’ – GGACCTTTGCACTTGTCGAGAATCG – 3’	5’ – GAGTCTCTCTTCTCTTGAGTCAGTG – 3’
FoxO	5’ – TAAGGATCCATGGTTGATAACG – 3’	5’ – TAAGAATTCTTAATGAACC – 3’
Hex	5’ – AAGGATCCATGTCGACTATACC – 3’	5’ – AAGAATTCTCAAGCATCTCG – 3’
Tel	5’ – GCTGCCACCAAAAGTCAGCT – 3’	5’ – GATGCCACAAAACAGACATCTC – 3’
Tgif	5’ – CACTTATTCTGGTTGTCTCCTGAGC – 3’	5’ – TTACGGTAAGGCATGGAATTGCCTGG – 3’

Table S2. Morpholino Sequences and Concentrations

Morpholino	Concentration	Antisense Oligo Sequence
LvDri1	2.0mM	5’ – GTAAAGTCTACAGACATTCGTTTGC – 3’
LvDri2	1.5mM	5’ – CGCGGTGGTTCACCCGAAAACCGAA – 3’
LvErg1	0.75mM	5’ – AATAATCACCAATCGTACACGACGT – 3’
LvErg2	0.5mM	5’ – GCTTTACTCAAAAGGCAGTCGGATA – 3’
LvFoxB1	0.3mM	5’ – CTGGTATTTCACAGAAAAGTCATGC – 3’
LvFoxB2	0.5mM	5’ – CCCCTTCTAAATAGATACAATGGTC – 3’
LvFoxO1	1.0mM	5’ – GGGTCGTTATCAACCATTTTGATGA – 3’
LvFoxO2	0.75mM	5’ – ATCCTAAATTGGGTCACAAGTACAC – 3’
LvHex1	2.0mM	5’ – TGCACGAACAAGTATCCAGAAATGC – 3’
LvHex2	1.5mM	5’ – GGTGCTGAACTTTACAAACAACTCT – 3’
LvTel1	0.75mM	5’ – ATCGTTCTTGGTCCTGGGCAGTTCC – 3’
LvTel2	1.0mM	5’ – ATGGTTCCTGGTCTTGTGAACCTGA – 3’
LvTgif1	0.5mM	5’ – ATCTTTCTTTTGATAAATCCGCATC – 3’
LvTgif2	1.0mM	5’ – CGTATGTTGACTTTTTCGCAGTGTT – 3’

Table S3. Sea urchin TFs required for EMT.

Sea Urchin EMT - TF	TF Family	Human Homologues TF Family Members	Vertebrate evidence of EMT relationship	Type of Evidence	Citation Examples
Alx1	Homeobox	ALX1 (CART1, FND3)	promotes EMT via SNAI1	direct	PMID: 23288509
		ALX3 (FND1)	upregulated in mesenchyme, craniofacial disorder	indirect	PMID: 23181698, 20534379, 9676189
		ALX4 (FND2)	gastric cancer metastasis, mammary cancer metastasis, craniofacial disorder	indirect	PMID: 22017425, 20145299, 11903336
Ets1	ETS (ETS subfamily)	ETS1 (ETS-1, EWSR2)	inhibits ECM production, required for neural crest EMT, breast carcinoma EMT	direct	PMID: 22829018, 17987123, 9247254
		ETS2	Upregulates MMP-2 in trophoblast invasion, breast cancer metastasis/invasion	indirect	PMID: 19939245, 9639404, 9500466, 16380248
Tel	ETS (TEL subfamily)	ETV6 (TEL, TEL/ABL)	myeloid malignancy, fusion protein in malignant leukemia	indirect	PMID: 22823977, 19287094
		ETV7 (TEL2, TELB, TEL-2)	B-cell malignancy, hematopoietic oncogenesis	indirect	PMID: 15743832, 16234363
Erg	ETS (ERG subfamily)	ERG (erg-3, p55)	overexpression induces EMT in prostate cancer	direct	PMID: 23027626, 21747944, 20713528
		FLI1 (EWSR2, SIC-1)	fusion protein in metastatic Ewing's sarcoma	indirect	PMID: 16204072, 9552022
		FEV (HSRNAFEV, PET-1)	fusion protein in metastatic Ewing's sarcoma	indirect	PMID: 17620387
Tbr	T-Box (TBR1 subfamily)	TBR1 (TBR-1, TES-56)	medulloblastoma	indirect	PMID: 22832583
		EOMES (TBR2)	loss blocks EMT	direct	PMID: 18171685
		TBX21 (T-PET, T-bet, TBET, TBLYM)	metastasis of gastric cancer	indirect	PMID: 22416188
Hex	Homeobox	HHEX (HEX, PRH, HMPH, PRHX)	mesenchymal cell expression after EMT induction, mailgnant haematopoiesiss	indirect	PMID: 21490434, 20676125
Tgif	TALE Homeobox	TGIF1 (TGIF, HPE4)	overexpression progresses urothelial carcinoma	indirect	PMID: 22771156, 22728270
		TGIF2	required for gastrulation, overexpressed in ovarian cancer	indirect	PMID: 20040491, 11006116
Snail	Snail	SNAI1 (SNAIL, SNAIL1)	overexpression induces EMT, E-cadherin repressor	direct	Reviewed in PMID: 23076049, 22945800, 17587826
		SNAI2 (SLUG, SNAIL2)	overexpression induces EMT, E-cadherin repressor	direct	Reviewed in PMID: 19273255, 21665887
		SNAI3 (SMUC, SNAIL3)	thyroid carcinoma	indirect	PMID: 22641097
Twist	Twist	TWIST1 (TWIST, bHLHa38)	overexpression induces EMT, E-cadherin repressor	direct	Reviewed in PMID: 19272800, 15640618
		TWIST2 (DERMO1, bHLHa39)	overexpression induces EMT, E-cadherin repressor	direct	PMID: 21602879, 22018873, 22103974
FoxB	Forkhead	FOXB1 (FKH5)	expression pre-neural crest delamination	indirect	PMID: 8861101
		FOXB2 (FKH4)	expression in developing spleen and thymus	indirect	PMID: 7689224
FoxO	Forkhead	FOXO1 (FKH1, FKHR, FOXO1A)	colorectal cancer, malignant parathyroid carcinoma	indirect	PMID: 21901254, 23001705
		FOXO3 (FOXO2, FKHRL1, FOXO3A)	promotes cancer cell invasion	indirect	PMID: 19564415, 21965295
		FOXO4 (AFX, AFX1, MLLT7)	required for neural crest migration	indirect	PMID: 19895805
FoxN2/3	Forkhead	FOXN2 (HTLF)	presomitic mesoderm	indirect	PMID: 12351180
		FOXN3 (CHES1)	neural crest development, craniofacial defects	indirect	PMID: 21050205, 17089409, 20691664
Dri	ARID	ARID3A (BRIGHT, DRIL1, DRIL3, E2FBP1),	oncogenic, promotes fibrosis, required for gastrulation	indirect	PMID: 11812999, 18583319, 15680369
		ARID3B (BDP, DRIL2),	malignant neuroblastoma, neural crest development	indirect	PMID: 22751132, 16951138, 16530748

Each TF in the sea urchin EMT GRN has at least one human homologue. 8 homologues have been directly implicated in vertebrate EMT. 22 homologues have not been assayed for EMT regulation but are expressed in a tissue where this is an EMT event. PMID = PubMed Identifier.